MASTER'S THESIS

MODEL-BASED EVALUATION OF DIFFERENT CONTROL STRATEGIES FOR THE VACUUM OXYGEN DECARBURIZATION PROCESS

executed at

Degree Program
Information Technologies and Business Informatics

Submitted By: Michael Mayer
Matriculation Number: 1610320034

Graz, December 15, 2017 .....

Michael Mayer

Preface

I declare that I have authored this thesis independently, that I have not used other than the declared sources and resources, and that I have explicitly marked all material which has been quoted either literally or by content from the used sources.

.....

Michael Mayer

Acknowledgments

Firstly, I would like to thank my thesis supervisor Dr. Johannes Hatzl. There was always time for an answer whenever I ran into a trouble spot or had a question about my research or writing. In particular I want to thank Dr. Hatzl for many insightful conversations during the development of the thesis, his vast knowledge where I gained from and the extremely useful comments.

I would also like to thank my appreciated colleague and expert who was involved in this research: Dr. Robert Pierer. Without his passionate participation and input regarding the fundamentals of metallurgy and modeling, the examination and study of the process model could not have been successfully conducted.

Finally, I must express my very profound gratitude to my parents and to my spouse for providing me with unfailing support and continuous encouragement throughout the numberless busy weekends of study besides the full-time job and through the process of researching and writing this thesis. This accomplishment would not have been possible without them. Thank you.

Michael Mayer

Graz, December 15, 2017

Abstract

The importance of stainless and special steel products has increased substantially in recent decades, as their use has shifted from niche special applications to widespread popular function. Clearly, the vacuum oxygen decarburization (VOD) process plays a major role in stainless steel production. In order to achieve extremely low carbon ratios in the presence of high chromium content, oxygen is blown under reduced pressure conditions. Despite the well-known determination of the required amount of oxygen, the operation practice itself seems to vary in the field. This gives rise to the question of the existence of a consistent optimized control strategy.

The present master's thesis addresses the existing optimization problem by using a multiple-validated VOD process simulation model. As a first step, the optimization problem is defined by the examination of the existing model. Thus, the process model flow is step by step transformed into mathematical terms. Subsequently, a variable study is carried out evaluating the influences of the oxygen blowing rate, stirring gas rate and the system pressure on the result of the model. Based on the findings, an optimization algorithm is then implemented to generate enhanced control strategies with respect to the given optimization criterion: minimize chromium oxidation. Finally, the results are demonstrated by simulations and tests of generated control strategies with the existing model. These tests clearly show an improvement regarding the optimization criterion. Moreover, the results demonstrate numerically and visually, that the newly developed algorithm generates enhanced control strategies.

Zusammenfassung

Die Bedeutung von Edelstahl- und Spezialstahlprodukten hat in den letzten Jahrzehnten erheblich zugenommen, da sich ihre Verwendung von speziellen Nischenanwendungen zu einem Massenprodukt verlagert hat. Das Vakuum-Sauerstoff-Entkohlungsverfahren, engl. Vacuum Oxygen Decarburization (VOD), spielt eine wichtige Rolle in der Edelstahlproduktion. Um die für Edelstahl notwendigen niedrigen Kohlenstoffraten unter Berücksichtigung des hohen Chromgehalts zu erreichen, wird Sauerstoff bei reduzierten Druckverhältnissen aufgeblasen. Obwohl die Berechnung der benötigten Sauerstoffmenge bekannt ist, sind die Blaspläne für den VOD Prozess selbst in der Praxis verschieden. Daraus resultiert die Frage nach einem möglichen konsistenten und optimierten Behandlungsplan.

Diese Masterarbeit befasst sich mit dem zugrundeliegenden Optimierungsproblem unter Verwendung eines mehrfach validierten VOD-Prozesssimulationsmodells. In einem ersten Schritt wird das Optimierungsproblem durch die Untersuchung des bestehenden Prozessmodells definiert. Für die Definition ist es notwendig, den Prozessfluss des Modells Schritt für Schritt in mathematische Formulierungen zu transformieren. Anschließend werden in einer Variablenstudie die Einflüsse der Sauerstoffblasrate, der Spülgasrate und des Systemdrucks auf das Ergebnis des Modells bewertet. Auf Basis der Ergebnisse der Variablenstudie wird ein Optimierungsalgorithmus implementiert, um verbesserte Blaspläne in Bezug auf das gegebene Optimierungskriterium zu erzeugen: minimale Chromoxidation. Abschließend sind die Ergebnisse durch Simulationen und Tests generierter Blaspläne mit dem vorhandenen Modell dargestellt. Diese Tests zeigen eine deutliche Verbesserung hinsichtlich des Optimierungskriteriums. Darüber hinaus demonstrieren die Ergebnisse sowohl numerisch als auch graphisch, dass der neu entwickelte Algorithmus verbesserte Blaspläne generiert.

Contents

1 Introduction

Over the last decades, but especially since the beginning of the twenty-first century, the global demand for stainless steel faced a significant increase. According to the International Stainless Steel Forum, which annually provides the latest facts and figures, the world's stainless steel production has increased to a volume of 45.8 million metric tonnes in the year 2015 compared to 1 million metric ton back in 1950. The major increase was seen in the Asian market, whereas the European as well as the American stainless steel production remained stable.

To understand the increase of demand for stainless steel, it has to be mentioned that stainless steel applications have shifted from less special use-cases to many various areas of applications. Out of many examples of stainless steel applications, taken from a publication of the British Stainless Steel Association (n.d.), the following is one of the most important buildings for the modern Europe: the European Court of Human Rights in Strasbourg. The building was finished in 1995 and consists of two cylindrical chambers, one for the European Commission and the other for the European Court itself. Both chambers are clad in stainless steel. Another more extraordinary example is the *Murinsel Graz*, which is small artificial island in the river Mur, build by the city of Graz originally designed for hosting the European Capital of Culture back in 2003. However, meeting the wish of locals, the island has not been deconstructed until now. Without stainless steel this would not be possible, since the important glass nodes of the island are made of stainless steel and the walkway has a stainless steel mesh.

Referring to the increase of demand, the stainless steel production has become critical in order to finally meet the increased demand. In this case, critically refers to productivity and costs. In general, the argon oxygen decarburization (AOD) process and the vacuum oxygen decarburization (VOD) process plays the key role along the stainless steel production route. Both processes rely on the metallurgical know-how of those who produce

the steel. Consequently, nowadays many steel producers perch on software systems to support the process and to make it more cost efficient. The present master's thesis focuses on the VOD process and the metallurgical operation of it. Based on a modeling software, which is installed and accepted in the field, the thesis decomposes the VOD process into its single steps and identifies the influences on the results of the model. Finally, based on the model the thesis evaluates mathematical optimization possibilities.

1.1 Motivation

The roots of the research concept of the present master's thesis are the prevalent challenges and requirements of INTECO melting and casting technologies GmbH, an Austrian supplier for steelmaking and special steelmaking solutions. Hereby, the prevalent challenges are often hidden the supply of solutions, compared to the equipment-supply only concept. In other words, INTECO does not only supply the equipment for the steel- and special steelmaking industry but offers also proven metallurgical know-how to operate these types of equipment. Moreover, customers from all over the world have the possibility to purchase application-specific know-how bundled in a software-suite named INTECO Metals Application Suite (IMAS). Explained by using the classical automation pyramid, IMAS covers typical level 2 and level 3 functionality of the manufacturing industry. In domain-specific literature, level 2 is often referred to process automation, whereas level 3 often means plant automation or manufacturing execution systems (MES). As part of the process automation functionality of IMAS, the software system provides metallurgical models. As mentioned above, such models provide guidance and know-how in order to support customers using this software. Metallurgical models, often based on a combination of physics and empiricism, are incorporated for various steelmaking processes. In terms of the VOD process, a real-time model has been developed to predict the current state of the production at every time. The requirements and prerequisites of VOD process itself together with the presence of a validated and accepted real-time model is the origin of the present research. Undoubtedly, further improvement of the software services in order to provide better solutions for their customers is the main driving force of INTECO for researches in the field of modeling.

1.2 Problem Statement

Based on the fact, that the AOD and the VOD process are the dominant methods for producing high-chromium anti-corrosion steel grades, the problem statement of the present master's thesis focuses on the treatment of the VOD process. In particular, on the know-how concept of operating the VOD process. Therefore, a brief introduction into the AOD and VOD background is necessary. Generally speaking, both processes aim to reach low carbon contents among the chemical composition of the steel. Typical stainless steels have no higher carbon concentration in the final product than 0.12 %. AOD and VOD are generally based on oxidation of carbon in the metal bath by injecting oxygen. Thereby, the oxygen is blown onto the metal bath by a water-cooled oxygen lance. In addition, both processes have methods to reduce the partial pressure of the system. By reducing the partial pressure, the carbon condition in equilibrium drops to much lower values. This in turn increases the reaction of carbon with oxygen. However, both processes pursue different approaches for the partial pressure reduction. While the AOD process reduces the partial pressure by injecting high amounts of argon inert-gas, the VOD process reduces the system pressure in the tank itself (Patil, Chan, & Choulet, 1998).

The present master's thesis focuses on the VOD process only, some cross-references to the AOD process are pointed out due to the similarities. The VOD process starts based on the current chemical composition of the steel before any decarburization. Based on the amount of carbon, the required amount of oxygen based on oxidation can be calculated. The calculation needs to consider as well the oxidation of so called priority elements: Al, Ti and Silicon. The order of oxidation can be either determined by the complex Gibbs minimization or obtained by the Richardson-Ellham diagram for constant temperature and pressure (Patil et al., 1998). Hence, the calculation determines the minimum required amount of oxygen to reduce the carbon content to a certain controlled target. During the injection of oxygen through the lance, the system pressure can be reduced to a level around 200 mbar. Due to heavy turbulence, the equipment is the limiting factor. After injection of oxygen, the pressure will be finally reduced to a deep-vacuum level around 0.5 - 1 mbar. This condition will be hold for a certain amount of time and is called vacuum carbon deoxidation (VCD). Thus, the dissolved oxygen in the metal bath reacts with carbon to carbon-monoxide (CO), based on the lower pressure conditions (Choudhury, Bruckmann, & Scholz, 1988). In domain language, sometimes the term

boil-off is used to describe the same phenomenon. The boil-off phase is used to finally reach the carbon target concentration required (Reichel & Szekely, 1995).

1.3 Aims and Hypothesis

Based on the calculated amount of oxygen, there exist various patterns to operate the equipment in the field. The oxygen-blowing pattern is a diagram of the set-points system pressure [mbar], oxygen injection rate [$m^3\,h^{-1}$], stirring gas rate [$L\,min^{-1}$] over the process time [min] on the x-axis. In the field, this pattern is mainly created by metallurgists and process engineers. Starting from the experience of INTECO, the basis of the present thesis is the situation, that various oxygen-blowing patterns exist in the field. Thus, the aim of INTECO is to provide a smart software service in IMAS to generate practicable oxygen-blowing patterns for the VOD process. Besides, a generated pattern should consider a low cost strategy, based on the results of their existing VOD process model. The low-cost criteria comes from the unwanted oxidation of chromium. At this point, it comes to the even more complex topic of modelling metallurgical processes.

In modeling of metallurgical processes, especially the VOD process, challenges come up by multiple simultaneous occurring physical and chemical phenomena. And, to be as close to reality as possible, none of them can be neglected. Implicitly, these considerations lead to complex mathematical formulations of the overall system. Moreover, the interactions between single phenomena play an important role since they influence themselves mutually. However, besides the obvious complexity of modeling metallurgical processes, at the end all of them are subject to law of physics or thermodynamics. This leads to the question of a smart generation of an oxygen-blowing pattern, which is independent of the experience of the metallurgist and process engineer but based on the laws of physics and thermodynamics.

In order to do so, the first step has to be the understanding of the process itself. At second, a deeper knowledge about modeling in the field of steelmaking needs to be understood. At last the validated and accepted VOD model has to be examined in order to detect any possibility for optimization. Therefore, it is critical to illustrate the influence of different control-strategies and their mutual comparison. Therefrom, the research questions can be deduced:

1. What are the influences on the existing VOD model in terms of the chromium-oxidation?

2. Based on the findings of the influences, up to what specific point a mathematical optimization of the problem is possible?

On the one hand, the thesis aims to describe the definition of the optimization problem itself. This comes along with the identification of the influences of the variables on the model. On the other hand, the thesis aims to illustrate possibilities to mathematically optimize the oxygen-blowing pattern, based on the influences and findings beforehand. The accepted and validated VOD process model not only provides the information to understand the criteria and the phenomena, but serves also as validation of any oxygen-blowing pattern generated.

Consequently, the thesis' hypothesis and alternative hypothesis can be formulated as:

1. The examination and analysis of an existing and validated process model leads to an optimization algorithm to create enhanced VOD control strategies in terms of chromium oxidation.

2. The examination and variably-study shows, that an optimization based on a theoretical model is not sufficient due to the lack of physical phenomena and metallurgical experience.

1.4 Outline and Main Results

The present section provides a brief overview of the thesis' content together with a short summary respectively. In general, the focus of the research is the definition the optimization problem. Consequently, this definition serves as basis for the development of an optimization algorithm. The algorithm can be feed with the steel information before VOD and generates a control strategy. Thus, the following outline to the thesis applies:

1. Related Work
   The Chapter Modeling the Vacuum Oxygen Decarburization Process provides the

necessary background information. As a first step, the important metallurgical background for the VOD process is described followed by an introduction to modeling. This servers as basis for the main section of the chapter: the fundamental description of the existing model based on physics, thermodynamics and chemical backgrounds.

2. Optimization Problem

   The initial research work focuses on the definition of the optimization problem based on the fundamental backgrounds of the model. Therefore, constants, the variables, the objective function as well as constraints are defined. These definitions provide the basis for the following chapters. The objective function can verbally summarized as the minimization of the chromium oxidation.

3. Variable-Study

   As a first step of the variable-study, a numerical example is used to describe all the steps required to calculate the result of the objective function. With this information, the influences of the different variables on the result are examined. Thus, different solutions for the variables are simulated with the process model and the results evaluated. The study points out that a step-wise reduction of the oxygen-blowing together with the system pressure at the end of the blowing phase lead to less chromium oxidation. However, the study also shows that the stirring gas rate does not have a big influence, according to the existing model.

4. Optimization Algorithm and Numerical Tests

   Based on the findings of the variable-study and the mathematical problem definition, an algorithm to generate enhanced patterns has been developed. Detailed explanations of the algorithm are provided. The generated patterns based on the numerical example of the variable-study are simulated and the results are discussed. Finally, real data from the field is simulated and the original treatment is compared to the theoretical generated pattern. Clearly, the simulations and numerical tests points out that the newly developed model-based algorithm creates enhanced control strategies. Enhanced always refers to the optimization criterion: minimize chromium oxidation. This chapter also demonstrates the improvements in terms of comparable figures and graphical comparisons between the real carried-out blowing patterns and their optimized counterparts.

At last, in the conclusions of the thesis a summary of the research and the discussions of the main results are covered. The important finding to mention is that every result measured is according to the model, since the algorithm is directly derived from the existing model. Thus, there may be metallurgical phenomena not considered, which do have an effect in the real operation. Conversely, according to the current design of the model, the generated patterns of the algorithm show a theoretical improvement in terms of chromium oxidation.

2 Modeling the Vacuum Oxygen Decarburization Process

In order to face the increasing stainless steel demand, the argon oxygen decarburization (AOD) and the vacuum oxygen decarburization (VOD) processes are the dominating methods in nowadays stainless steel production. The development of the AOD process was a breakthrough in stainless steel production due to the significant lower production costs. When it comes to extremely low carbon stainless steels, almost every production route (so called duplex and triplex routes) ends with a vacuum treatment. As a result, the VOD process developed in Germany has become an important factor in order to reach low carbon contents together with the appropriate hydrogen and nitrogen adjustment (Fruehan, 1998). The discipline of modeling helps to get a better understanding of steelmaking processes. Since observations and permanent measurements are not possible, modeling has become a powerful tool (Brooks, Dogan, Alam, Naser, & Rhamdhani, 2011).

The present chapter describes the setup of a computational model simulating the VOD process. Therefore, dedicated metallurgical and modeling background sections provides related information. At last, the model setup is described in terms of building separate blocks and how these blocks interact.

2.1 Metallurgical Background

Both main decarburization processes (AOD and VOD) aim to reach low carbon contents by oxidation. During the oxidation at temperatures around 1600 to 1700 °C, alloying elements will be oxidized as a side effect. In particular these elements are aluminum, titanium, silicon but also chromium. Especially the latter leads to high costs due to the

necessity of additional reduction material. Consequently, steelmakers strive for minimizing the chromium oxidation. Therefore, different metallurgical strategies can be applied: (1) high temperature, reduced partial pressure due to (2) dilution or (3) vacuum (Fruehan, 1998).

The first one was used in electric arc steelmaking before any duplex or triplex production came up. Operation at higher temperatures favor carbon oxidation over chromium oxidation but leads to higher operational risks and refractory costs. The AOD process has introduced the dilution approach. Injecting argon or nitrogen gas lowers the partial pressure of CO p_{CO} in liquid steel. Further, the lowered partial pressure moves the equilibrium towards higher chromium contents and lower carbon contents. Similarly to AOD, the VOD process also uses the effect of lowering the CO partial pressure by reducing the tank pressure. Compared to AOD, the advantage of the VOD process is to reach extremely low carbon levels with the presence of high chromium contents and low argon consumption. The lower the chromium oxidation, the lower the additional costs for recovering chromium from chromium-oxide in the slag area (Ghosh, 2000; Deo & Boom, 1993; E. T. Turkdogan, 1996).

2.2 Modeling Background

In general, the term modeling defines a scientific representation of a process or phenomenon by a physical system or mathematical expressions. In this context, physical modeling investigates a given phenomenon in replica of the actual industrial unit. Thus, a physical model represents the system in smaller scale and sizes and often changed material. Since the present master's thesis focuses on mathematical modeling only, the interested reader is referred to relevant literature for physical modeling (e.g. Mazumdar & Evans, 2009). Mathematical modeling, compared to physical modeling, uses a set of equations and expressions in order to represent a specific phenomenon or process as close as possible. It is often used to predict certain phenomena without the necessity of physical replica and expensive experiments. Nowadays, the technique of modeling is well-established and demonstrates its capabilities in a wide range of applications in modern steelmaking. Mathematical models may range from empirical to fundamental models. The results of a model must always be seen in context to what extent the physics of the process has been incorporated in the formulation (Mazumdar & Evans, 2009). Mazumdar

and Evans (2009) also describe, that the term "model" often implies that relationships considered in mathematical expressions may not be quite exact.

Steelmaking processes tend to be very complex, since they involve several simultaneously occurring phenomena. These are heat, mass transfer, multiphase turbulent flow as well as chemical reactions among metal, slag, solid and gas (Mazumdar & Evans, 2009; Brooks et al., 2011). Additionally, such processes are highly transient, so that commonly used steady-state assumptions are often invalid (Brooks, Rhamdhani, Coley, & Pan, 2009). Because of the physical complexity of many metallurgical processes, it is often not possible to describe completely rigorous mathematical models based on fundamental physics and chemistry. However, the development of practical models for complex processes depends on making a compromise between the required detail, available data and information and the given limits of mathematical tools. Moreover, the acceptable time to find a solution is another factor (Himmelblau & Bischoff, 1968). The latter is key for online process simulation, which means the model evaluates the prevalent conditions in real-time. Online evaluation of such models often requires numerous idealizations or at least some basic assumptions in order to reduce the complexity. This leads to the combination of fundamentals and empiricism for practical efficient models (Mazumdar & Evans, 2009).

Out of various modeling techniques, for example Brooks et al. (2011) classify the most common techniques into three groups: (1) computational thermodynamics, (2) computational fluid dynamics (CFD) and (3) computational kinetics. Computational thermodynamics models are used to determine the impurities distribution among phases and help to understand the limits of the system. CFD describes fluid flow patterns and phase interactions within the system. At last, computational kinetics calculates concentration changes within and among the phases over time. The phenomena covered by thermodynamics, kinetics and fluid dynamics are strongly interrelated. Thus, the modeling techniques interact as well, such as the results of CFD models provide important parameters to understand convective mass transfer. Likewise, computational thermodynamics evaluate the limits for computational kinetic modeling. Over the last decades, the steadily increasing availability of more powerful computers has reduced the calculation time of CFD. Nevertheless, such models are still rarely used for real-time modeling up to now. This clearly indicates the complexity of simulating dynamic flow patterns. Thus, the present thesis focuses on computational thermodynamics and kinetics, which are the fundamentals of

the existing VOD model. The following two subsections summarizes these two modeling techniques briefly. For the sake of completeness, other phenomena, like heat and mass transfer as well as the behavior of gas jets in liquid, play also an important role during secondary steelmaking. Moreover, the following two subsections represent partially fundamental physics, which is not cited explicitly. Major content is based on the the publication of Brooks et al. (2011) and are supplemented by relevant domain specific articles and textbooks (Ghosh, 2000; Deo & Boom, 1993; E. T. Turkdogan, 1996; Fruehan, 1998; Rodríguez-Hernández, Garnica-González, & JA, 1997).

2.2.1 Computational Thermodynamics

The discipline of thermodynamic modeling enables the determination of the equilibrium conditions of elements among the phases. Thermodynamics also evaluates the energy generated or consumed by chemical reactions and behavioral changes of elements in solution. The fundamental of all the computational thermodynamics used in the present thesis is the second law of thermodynamics. There are various statements of the law, but the first formulation is credited to the French physician and engineer Nicolas Léonard Sadi Carnot in 1824. Simplified, the second law of thermodynamics describes that the entropy in a cyclic process can either increase or remain the same. The latter is a steady-state condition, which is also called equilibrium (Buchdahl, 2009). The Gibbs free energy minimization of the system at constant temperature and pressure, which is developed from that law, is a well-established technique to conduct equilibrium calculations (Wulandari, Brooks, Rhamdhani, & Monaghan, 2009):

$$\begin{aligned} G &= \sum_i n_i \cdot \mu_i \\ &= \sum_i n_i \cdot \left(\mu_i^0 + R \cdot T \cdot \ln a_i\right) \rightarrow \min \end{aligned} \tag{2.1}$$

The present formulations are the fundamentals of the Gibbs free energy minimization. The variables contained are the gas constant R, temperature T, mole fraction of element n_i and μ^0 identifies the standard chemical potential. Finally, the equations use another important parameter of thermodynamics: the activity of element a_i. Activity in thermodynamics can be perceived as "effective concentration" of particular elements. It is an important way to quantify how elements dissolve into each other. In thermodynamic modeling, the phases and elements within the phases needs to be defined carefully in order

to describe a system. Moreover, each element defined in the model requires appropriate thermochemical data before any technique like the Gibbs free energy minimization can be applied. Thermochemical data includes for example heat capacity, enthalpy or entropy, defined as function of temperature for each element. For that purpose, international recognized institutes such as the National Physical Laboratory (NPL) and the National Aeronautics and Space Administration (NASA) provide critically evaluated large databases for thermochemical data. For equilibrium calculations itself, there are widely used software packages like Thermodata, Factsage, Thermo-Calc, MTData, HSC, Chemix or Gemini2 available (Wulandari et al., 2009; Gordon & McBride, 1994; Gaskell, 2008; Eriksson, 1975; Gaye, Lehmann, Rocabois, & Ruby-Meyer, 2001).

The determination of an applicable solution model for each phase of the model is another key challenge in computational thermodynamic modeling. In steelmaking processes, the system usually contains the phases liquid steel, slag and in case of electric arc steelmaking also solid scrap. In case of the liquid iron phase, a dilute solution model is well established. This model uses empirically deduced interaction parameters to calculate the activities of the species. Henry's Law forms the basis for the dilute solution model by stating the activity of species is linear to their concentration. Considering deviations from Henry's Law at higher concentration levels and influences of other solutes the mathematical formulation is as follows (Henry, 1823):

$$h_i = f_i \cdot w_i \tag{2.2}$$

The formulation expresses Henry's activity h of each element i, whereas the f_i represents the activity coefficient at one weight percent standard state. Thus, the coefficient needs to be multiplied by the actual weight percent w_i. The activity coefficient describes the influence of one solute element to the activity of another. The mathematical expression of the activity coefficient can be described as:

$$\log f_i = \sum_k e_i^k \cdot w_k + e_{2i}^k \cdot w_k^2 + e_{3i}^k \cdot w_k^3 \tag{2.3}$$

The variable e_i^k is the interacting parameter, which describes the influence of solute k on the activity coefficient f of solute i. For most of the solute elements the second and higher order terms can be neglected. Among the literature, the interacting parameters

often vary. The present model incorporates the interacting parameters introduced in the publication of Kleimt et al. (2006).

In oxygen steelmaking and secondary refining, such as the vacuum oxygen decarburization process, the most important reaction is between elements and oxygen. This chemical reaction can be defined in a generic way:

$$a[i] + \frac{b}{2}\mathrm{O}_2 = (i_a\mathrm{O}_b) \tag{2.4}$$

The expression describes the oxidation of a given element i to a resulting oxidized product. The variables a and b are used to balance the chemical reaction. Exemplary, Equation (2.4) is used as follows (E. Turkdogan & Fruehan, 1998):

$$\begin{aligned} 2[\mathrm{Al}] + \frac{3}{2}\mathrm{O}_2 &= (\mathrm{Al}_2\mathrm{O}_3) \\ 2[\mathrm{Cr}] + \frac{3}{2}\mathrm{O}_2 &= (\mathrm{Cr}_2\mathrm{O}_3) \\ [\mathrm{C}] + \frac{1}{2}\mathrm{O}_2 &= \{\mathrm{CO}\} \end{aligned}$$

In case of carbon oxidation, the product in the parenthesis (CO) must be replaced by their gas-phase representing equivalents $\{\mathrm{CO}\}$.

For the activity distribution in slag components, however, the modeling of the solution is more challenging. The reason is the difficulty of the description of the complex molecular structure of slag components (e.g. Aluminum-oxide $\mathrm{Al}_2\mathrm{O}_3$). A further reason is the lack of knowledge in the community about the interaction of different metal oxides in the slag (Ekengård, 2004). Cross-references in the publication of Brooks et al. (2011) indicate several researches and developments of models for multi-component oxide systems. Such models include complex ionic two sub-lattice, regular solution, associated solution and modified quasi-chemical expressions. By reviewing the relevant literature, the following three models are generally in use:

1. Ohta and Suito slag model
2. ThermoSlag (KTH-model)
3. Irsid slag model

The slag model introduced by Ohta and Suito (1998) represents empirical equations based on experimentally determined activity data at 1600 °C. The data was obtained by using a slag-metal equilibrium technique. The suggested formulations for the activities of the slag composites $\mathrm{Al_2O_3}$ and $\mathrm{SiO_2}$ as well as the activity coefficient of MnO and FeO are summarized in the following list of equations:

$$\log a_{\mathrm{Al_2O_3}} = \frac{-0.27 \cdot w_{\mathrm{CaO}} + 0.167 \cdot w_{\mathrm{MgO}}}{w_{\mathrm{SiO_2}}} + 0.033 \cdot w_{\mathrm{Al_2O_3}} - 1.56 \tag{2.5}$$

$$\log a_{\mathrm{SiO_2}} = 0.036 \cdot w_{\mathrm{MgO}} + 0.061 \cdot w_{\mathrm{Al_2O_3}} + 0.123 \cdot w_{\mathrm{SiO_2}} - \frac{0.595 \cdot w_{\mathrm{SiO_2}}}{w_{\mathrm{CaO}}} - 6.456 \tag{2.6}$$

$$\log a_{\mathrm{MnO}} = 0.019 \cdot w_{\mathrm{CaO}} + 0,023 \cdot w_{\mathrm{MnO}} - 0.023 \cdot w_{\mathrm{SiO_2}} + 0.129 \tag{2.7}$$

$$\log a_{\mathrm{FeO}} = \frac{0.676 \cdot w_{\mathrm{MgO}} + 0.267 \cdot w_{\mathrm{Al_2O_3}} - 19.07}{w_{\mathrm{SiO_2}}} + 0.0214 \cdot w_{\mathrm{CaO}} - 0.047 \tag{2.8}$$

The ThermoSlag (previously called KTH model) represents a semi-empirical model for the calculation of thermodynamic properties in multi-oxide slag systems. The model describes high order slag systems by using experimental information from the binary subsystems. The description of oxide melts including silicate solutions as an O2- matrix is based on the relevant cations distributed. The model considers the interactions between cations, Fe2+, Ca2+, Mg2+ and Mn2+ together with Si4+ in the presence of oxygen. These basic cations distort the oxygen matrix and arrange the ionic melt (Björkvall, 2000).

The Irsid slag model can be used in combination with the database of ThermoCalc. The model formalism is based on a description of the slag structure originally suggested by Frohberg and Kapoor (1978). The silica melts are built upon symmetric and asymmetric cells composed of one oxygen ion surrounded by two cations of either the same or a different kind (Gaye & Coulombet, 1984).

2.2.2 Computational Kinetics

Whereas thermodynamic modeling evaluates equilibrium conditions of steelmaking reactions, it does not give any answer about how fast these reactions happen neither what influences their rate. As another field of research, the so called "reaction kinetics" endeavors to answer these questions. Brooks et al. (2011) refer in their publication the term "reaction kinetics" to the overall reaction process, whereas other publications may use it to describe the molecular reaction speed only. For this purpose, Brooks et al. (2011) introduce the term "inherent kinetics" to refer to the actual molecular re-arrangement procedure. The present thesis follows this terminology. In order to describe the difference between reaction- and inherent kinetics, the dissolution process of sugar in a tea cup can be used. For the sugar dissolution rate, the diffusion plays an important role. Whilst stirring the cup does not increase the inherent kinetics it accelerates the diffusion due to increased mixing. Compared to computational thermodynamics, the field of computational kinetics is less researched. This includes a lesser availability of knowledge databases and commercial software (Brooks et al., 2011). The present sub-section provides a brief introduction to fundamental kinetics, as needed to follow the used model in this thesis.

In steelmaking operations, inherent kinetics are less important in limiting reaction rates due to high temperatures. It is more the transfer of elements within phases which controls the rates. In general, the basis for predicting reaction rates in steelmaking operations is Fick's first law. The law describes that the diffusion rate is proportional to the concentration gradient and can be formulated as follows (e.g. E. Turkdogan & Fruehan, 1998):

$$J = -D\left(\frac{\partial C}{\partial x}\right) \tag{2.9}$$

in which J defines the mass flux in the direction defined as x ($\mathrm{mol\,m^{-2}\,s}$). D is the diffusion coefficient ($\mathrm{cm^2\,s^{-1}}$) and the variable C is the elements molar concentration involved ($\mathrm{mol\,m^{-3}}$). The discretization of models over the time can help to reduce the complexity. In this context, time is often introduced as the differential variable in the equation. Thus, according to Brooks et al. (2011) Equation (2.9) can be simplified to:

$$\frac{dC}{dt} = k \cdot \frac{A \cdot \rho}{m} \cdot (C_{act} - C_{eqm}) \tag{2.10}$$

In Equation (2.10) the variable k refers to the total mass transfer coefficient. In order to follow Fick's law the interface area A is divided by the volume, represented by ratio of steel density ρ and total steel mass m. The difference between the actual concentration C_{act} and the equilibrium concentration C_{eqm} describes the element involved in the reaction. The challenges in using Equation (2.10) are the determination of either the interface area A or the mass transfer coefficient k. As an example, k strongly depends on the prevailing conditions of each system the model is applied to. In case of steelmaking, the variable varies with stirring conditions, the multi-oxide slag phase weight and composition or temperature accompanied by others (Hallberg, Jonsson, & Jönsson, 2004). Since both parameters are related to the rate of turbulence energy dissipation, estimates may be made from the turbulence theory. In the field of modeling decarburization under reduced pressure, Reichel and Szekely (1995) suggest to introduce an overall exchange coefficient β:

$$\beta = k \cdot \frac{A \cdot \rho}{m} \tag{2.11}$$

The dimension of β is s^{-1}. Thus, many studies introduced it as time constant or reaction time in Equation(2.10) which can act as parameter for model adjustments. Besides the determination of A and k, it must be stated that reducing Fick's first law to the first order differential Equation (2.10) involves a lot of simplifications. In order to describe the gross simplifications, Brooks et al. (2009) has addressed these issues through transient kinetic theories. As part of these theories, they describe the creation of metal droplets in oxygen steelmaking processes, which are ejected to the emulsion phase due to oxygen injection. Importantly, the droplets spend time in emulsion before falling back to the metal bath. As a result, ejected droplets in emulsion increase the reaction area significantly and consequently the reaction rate increases.

Although many referencing models introduce empirical relationships, it obviously shows the complexity of oxygen steelmaking processes. Clearly, the complexity is transferable to fundamental-based modeling of such processes. According to the article of Brooks et al. (2011), the development of models is always a mixture of basic physics and empiricism. However, the mixture leads to useful results and understandings of the underlying phenomena. It will always be a balancing act between scientific rigor and practical results and solutions for a specific phenomena.

2.3 Fundamentals of the Existing Model

The following describes the physics, chemical equations and assumptions used for the existing computational model. The publication of Mayer, Pfennig, Weigl, and Pierer (2017) describes the engineered model for on- and offline simulation from the software development perspective. The fundamental backgrounds and physics of this model is mainly based on the pioneering work carried out at VDEh-Betriebsforschungsinstitut GmbH (BFI) Düsseldorf (Kleimt et al., 2006). In order to summarize the most important fundamentals of the used model, the present section is subdivided into an overview of the basic structure followed by modeling related sub sections.

2.3.1 Overview and Structure

Based on the backgrounds of the VOD process and considering computational modeling constraints, some assumptions for the existing model are comprised. Basically, the model covers two stages of the VOD refining process: (a) the oxygen blowing phase and (b) the vacuum carbon-deoxidation (VCD) or boil-off stage. In terms of phases, the model covers the metal/gas and the metal/slag reaction phases. The description of the construction and flow of the model is based on the schematic flowchart shown in Figure 2.1. The chart illustrates the data flow and calculation sequence of the separate model blocks. In other words, the entire model is portioned in sub-models. Importantly, the term sub-model and model block is used equivalent. The sub-models or model blocks are illustrated in fully transparent boxes, whereas data processing steps are shown with a gray pattern. Figure 2.1 also shows that the model itself is used as core, whereas the hosting environment makes sure to feed it with the correct data (Mayer et al., 2017). For every time-cycle, the prepared process data together with the current heat state is handed over to the model. From this point on, the computation follows the flow of model blocks shown in Figure 2.1.

Referring to the literature, many thermodynamic and kinetic models are classified as single-phase or multi-phase models (sometimes a phase is also termed as zone). Several developed single-phase steelmaking models can be found in the relevant literature (e.g. Lytvynyuk, Schenk, Hiebler, & Sormann, 2014), whilst modeling the AOD as well as the VOD process mainly uses the multi-phase approach. Furthermore, six types of dynamic

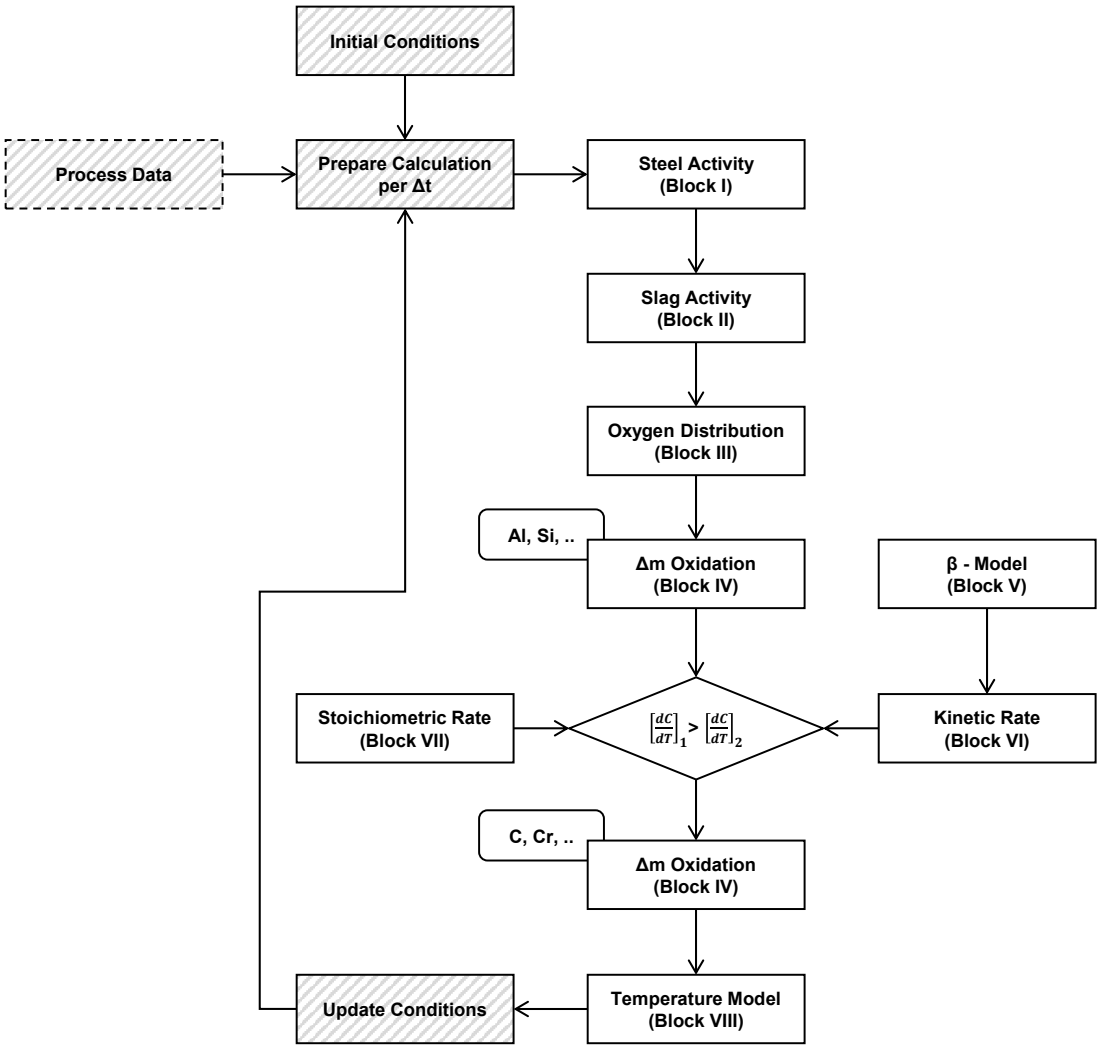

Figure 2.1: Schematic flow-diagram of the VOD model implementation

models for metallurgical process operating under reduced pressure can be distinguished (Ding, Blanpain, Jones, & Wollants, 2000):

1. Complex process mechanism model
2. Simple oxygen distribution ration model
3. Reaction interface model
4. System free energy minimization model
5. Empirical and statistical models

For a detailed description of these models the interested reader is referred to the publication of Ding et al. (2000). Besides the work of Kleimt et al. (2006) and Ding et al. (2000), the fundamental description of the model is also based on researches in the field of AOD and VOD, for example publications of Reichel and Szekely (1995), Wei and Zhu (2002), or Wei and Li (2015). Further and specifically referenced sources are cited explicitly.

In the following sub-sections, the different sub-models are described chronologically based on the explained calculation sequence followed by the description of the interrelation of the overall calculation cycle.

2.3.2 Thermodynamic Data

Throughout the entire VOD refining process (oxygen blowing and VCD) thermodynamic data is required. Most of the model blocks shown in Figure 2.1 require the activities and activity coefficients of the elements among the phases. Therefore, the steel activities and slag activities must be calculated and provided. This leads to the first and second sub-models:

1. **Steel Activity Calculation** (Sub-model I)
   In general, the calculation of the activity of elements within the metal phase are based on Henry's law (see Section 2.2.1). In order to conduct the activity coefficients necessary for the activity calculation, the interaction parameters published in the model of Wagner (1952) were taken in first place. However, it is also well-known that this approach should only be used in a dilute solution model (even if second order or higher interaction parameters are considered). This means the content of elements like Al, Si, C, Cr, Ni or Mn are nearly zero percent, whereas the content of Fe is almost one hundred percent. Regardless, many publications use the approach without any further adaption. To reduce the inadequacies for high alloyed stainless steel, the model uses the interacting parameters published by the Japanese publication of Sourcebook (1988). Finally, some modifications are made regarding the O, C and Cr interacting parameters based on the article of Kleimt et al. (2006). The modified parameters are selected with respect to the decarburization process of high-chromium steels (Otto, 1976). For providing activities and activity coefficients, Equations (2.2) and (2.3) are used. The second order term is considered for the activity coefficients of C and Cr.

2. **Slag Activity Calculation** (Sub-model II)

   Due to the fact that no practicable solution has been found in the integration of commercial software packages like ThermoCalc or the Irsid slag model, the empirical equations suggested by Ohta and Suito (1998) have been incorporated in the model. However, the publication of Ohta and Suito (1998) do not provide a simple equation for the activity $a_{\mathrm{Cr_2O_3}}$ of chromium-oxide nor for the corresponding activity coefficient $f_{\mathrm{Cr_2O_3}}$. Thus, the model uses the following empirical equations for the chromium-oxide activity:

$$\begin{aligned} B &= \frac{x_{CaO}}{x_{SiO_2}} \\ N &= -0.4249 \cdot B^4 + 1.7879 \cdot B^3 - 2.6886 \cdot B^2 \\ &\quad + 1.5492 \cdot B + 1.3126 \\ A &= 2.9505 \cdot B^{0.6899} \\ a_{Cr_2O_3} &= A \cdot x_{Cr_2O_3}^N \end{aligned} \tag{2.12}$$

   This mathematical formulation is deduced based on descriptions and diagrams of the publication of Xiao and Holappa (1993).

2.3.3 Oxygen Distribution and Reactions

The previously described sub-models one and two are be typically categorized into computational thermodynamic models. Having these sub-models providing the basic thermodynamic properties for each calculation cycle, the next calculation steps can be described. For this purpose, the model comprised assumptions, which lead to the following next parts:

1. **Oxygen Distribution Model** (Sub-model III)

   Based on the physical process of oxygen blowing, the design of the model assumes that the oxygen injected on the metal bath reacts simultaneously with Al, Si, Ti, C, Cr, Mn and Fe. In order to distribute the injected oxygen amount between the mentioned elements, the Gibbs free energy must be calculated. By obtaining the Gibbs free energy for each element mentioned above, a ratio for each element can be computed. However, due to the complexity and the necessity of real-time modeling, the simultaneous oxidation using a Gibbs distribution was discarded for

Number	Parameter	Default Value
(1)	Ratio C	0.75
(2)	Ratio Cr	0.20
(3)	Ratio Mn	0.03
(4)	Ratio Fe	0.02
(5)	Yield Oxygen	0.8
(6)	Oxygen Dissolution	0.03

Table 2.1: Adjustment parameters for the oxygen distribution model

the implementation of the model. Instead, a simple solution is introduced by using simple input parameters for a basic distribution of C, Cr, Mn and Fe during the oxidation phase. Thus, the model further assumes that the oxidation of elements with a higher affinity to oxygen takes place before any C, Cr, Mn or Fe reacts. Considering the relevant interest on C, Cr and temperature at the end of the process, this approach does not effect the results of the model. Consequently, the model oxidizes Al, Si, Ti and Nb sequentially before the "main oxidation" phase. The sequence for oxidizing these elements is taken from the Ellingham-Richardson-diagram, which illustrates the temperature ΔG relationship of the reactants (Ellingham, 1944). The resulting sequence is ranked by the ΔG at a temperature of $1600\,^{\circ}\mathrm{C}$. The oxidation itself is part of a separate model block. Thus, the oxygen distribution block provides the parameters for the main oxidation phase only and can be obtained by Table 2.1. The model distributes the total amount of oxygen in a given calculation step by these ratios. This implies that the total amount of oxygen is known at this stage of the calculation. Hence, the oxygen distribution block is also responsible for providing the ΔO (kg), always considering the Δt (s) of the actual calculation cycle. Firstly, the determination of the ΔO amount requires the input parameters from Table 2.1. Secondly, the following equations can be applied:

$$\begin{aligned} \frac{\Delta O}{dt} &= \dot{O} \cdot \eta_O \\ \frac{\Delta m[O]}{dt} &= \frac{\dot{O} \cdot \eta_{O_{diss}}}{\rho_O} \end{aligned} \tag{2.13}$$

In other words, Equation (2.13) can be explained as: the variable $\dot{O}$ ($\mathrm{m^3\,s^{-1}}$) refers to the given oxygen injection rate; additionally, η_O and $\eta_{O_{diss}}$ refer to the parameters oxygen yield (No. 5) and oxygen dissolution (No. 6) from Table 2.1. The result for $\Delta m[O]$ is the assumed amount of oxygen dissolved in the metal bath. On the one hand, parameter (No. 5) often termed as yield describes the immeasurable loss of

oxygen through the process itself. This includes that oxygen is partially sucked off by the operation of an off-gas equipment during the process. On the other hand, parameter (No. 6) describes that a small portion of oxygen will not react among phases, but goes into solution of the metal phase.

2. Δm **Oxidation Block** (Sub-model IV)
   Each separate model block considers the results of the previous blocks. In case of the Δm oxidation block, the oxygen distribution model is used. In general, the Δm oxidation block evaluates the mass exchanges between the metal/gas or metal/slag reaction phases. This means, the mass of elements in the metal phase will be removed by the oxidized amount Δm_i. On the contrary, the mass of oxides in the slag phase increases by the formed Δm_j. The mathematical expressions to determine the delta mass of an element, which will be considered for oxidation in the current calculation cycle, are according to Equation (2.4) as follows:

$$\begin{aligned} \nu_i &= \frac{22.4 \cdot b}{2 \cdot a \cdot M_i} \\ \Delta m_i &= \frac{\Delta O_i}{\nu_i} \end{aligned} \tag{2.14}$$

   The value 22.4 used in Equation (2.14) refers to the ideal gas law, which states that one mole of a gas occupies 22.4 liters at standard temperature and pressure. The variable M_i is the molar mass of element i and Δm_i refers to the mass of oxygen remaining for element i based on the oxygen distribution block. Correspondingly, the resulting mass of oxides can be expressed as:

$$\begin{aligned} \nu_j &= \frac{M_j}{a \cdot M_i} \\ \Delta m_j &= \nu_j \cdot \Delta m_i \end{aligned} \tag{2.15}$$

   Similar to Equation (2.14) above, the variable M_j refers to the molar mass of the oxide component (e.g. SiO_2).

2.3.4 Stoichiometric and Kinetic Decarburization Approach

Based on the description of the last sub-section, the model will not oxidize any carbon or chromium until all the side elements are oxidized. Once these elements are oxidized, the reaction with carbon and chromium must be considered. By doing so, the following

assumption is essential: as long as the decarburization rate due to the stoichiometric equation is smaller than the kinetic decarburization rate, the total amount of oxygen reacts with carbon. If the decarburization rate due to the kinetic approach is less than the stoichiometric decarburization rate, the loss of carbon will be calculated using the kinetic approach. Consequently, the leftover oxygen additionally reacts with chromium. This transition is also called the critical point, where the rate of carbon transport becomes rate limiting (Reichel & Szekely, 1995). In order to conduct the decarburization rate comparison, the model implements the following blocks (the description in reverse order is consciously):

1. **Stoichiometric Rate Calculation** (Sub-model VII)
   The stoichiometric decarburization rate describes the mass loss due to oxidation as explained in Equation (2.14). In order to clarify the used vocabulary: the term decarburization means the oxidation of carbon ($i = C$) in the metal bath. In a mathematical way, the model formulates the calculation of the stoichiometric rate as follows:

$$\begin{aligned} \frac{dm}{dt} &= \frac{\Delta O}{\nu_C} \\ \dot{m}_C &= \frac{dm}{dt} \end{aligned} \tag{2.16}$$

   The decarburization subject to the conditions of Equation (2.16) is only valid until the following conditional expression is in favor of the stoichiometric rate $\left[\frac{dC}{dt}\right]_1$ on the left hand side (also illustrated in Figure 2.1):

$$\left[\frac{dC}{dt}\right]_1 > \left[\frac{dC}{dt}\right]_2 \tag{2.17}$$

   The right hand side means the kinetic rate $\left[\frac{dC}{dt}\right]_2$. The kinetic rate derivation is explained in the successive sub-model six.

2. **Kinetic Rate Calculation** (Sub-model VI)
   Basically, the kinetic decarburization rate of carbon can be calculate by using Equation (2.10). Besides the challenges regarding the calculation of β, the kinetic rate conduction essentially needs a value for the carbon equilibrium $\mathrm{C_{eqm}}$. Thus, the carbon equilibrium concentration at the reaction phase can be deduced from the equations describing the oxidation reactions of carbon and chromium in equilibrium

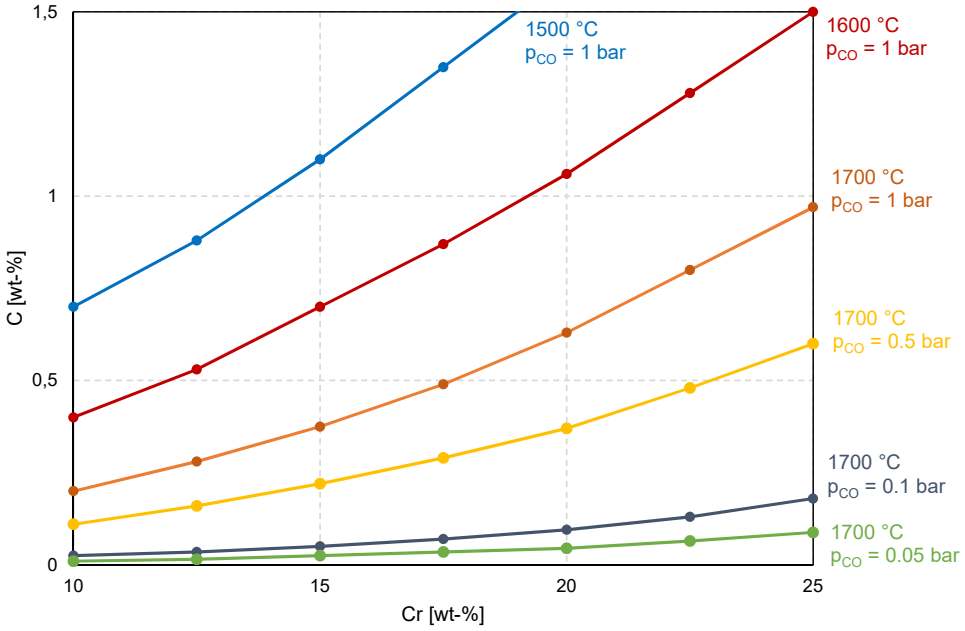

Figure 2.2: C-Cr relationship as function of pressure and temperature

conditions (Ding et al., 2000; Wei & Zhu, 2002):

$$\mathrm{C_{eqm}} = \frac{(f_{\mathrm{Cr}} \cdot \mathrm{Cr})^{2/3}}{f_{\mathrm{C}}} \cdot \frac{K_{\mathrm{Cr}}^{1/3}}{K_{\mathrm{C}}} \cdot \frac{1}{a_{\mathrm{Cr_2O_3}}^{1/3}} \cdot p_{\mathrm{CO}} \tag{2.18}$$

$$K_{\mathrm{C}} = 10^{\left(\frac{KA_{\mathrm{C}}}{KB_{\mathrm{C}}+T}\right)} \tag{2.19}$$

$$K_{\mathrm{Cr}} = 10^{\left(\frac{KA_{\mathrm{Cr}}}{KB_{\mathrm{Cr}}+T}\right)} \tag{2.20}$$

The activity and activity coefficients used in this equation are provided by the previously described thermodynamic model blocks one and two. The origin of the equilibrium constants are described in Equations (2.19) and (2.20).

In order to conduct the equilibrium conditions, the temperature cannot be neglected at this point. Next to the partial pressure of CO, the Equations 2.19 and 2.20 clearly point to a strong influence of the temperature on the Fe−C−Cr−O equilibrium. Many researches (e.g. Schürmann & Rosenbach, 1973; Heinen, 1997; Gmelin-Durrer, Trenkler, & Krieger, 1984; Lindenberg, Schubert, & Zörcher, 1987) referring in their publications to diagrams, which illustrate the critical carbon content over the chromium content as a function of p_{CO} and T. Figure 2.2 exemplary illustrates such a diagram and the mentioned correlations. According to Reichel (1996), the following conclusions can be made based on the diagram shown in Figure 2.2:

- Considering constant temperature and chromium content, lower carbon concentration can be obtained by low partial pressure of CO.
- The partial pressure of CO determines the stability of chromium-oxides. The lower p_{CO} at a given temperature, the lower is the stability of chromium-oxides.
- An increasing temperature of the metal bath results in the same effect as lowering the CO partial pressure: lower carbon contents can be reached without the oxidation of chromium.

To put it more general, the relationship can be summarized as follows: above a certain line in the diagram, the carbon oxidation is in favor; below the curves of the diagram, chromium will be oxidized preferably. For example, at a chromium concentration of 15 wt-% at atmospheric pressure, the lowest carbon content which can be reached without chromium oxidation is approximately: 1.1 wt-% at 1500 °C, 0.7 wt-% at 1600 °C and 0.37 wt-% at 1700 °C;

3. β **- Model Conduction** (Sub-model V)
   The β-model block refers to the relationship between the equations (2.10) and (2.11). In order to calculate β (see Equation 2.11), the mass transfer coefficient k and the reaction area A must be determined for each calculation step. According to T. Kitamura, Miyamoto, Tsujino, Mizoguchi, and Kato (1996), the reaction of oxygen with carbon take place:

   a) at the bath surface (in the following indexed with $Surf$),

   b) at the surface of the injected gas bubble (in the following indexed with Ar), and

   c) inside the bath;

   However, the model only considers the first two reaction sites and neglects the reaction of carbon with oxygen inside the steel bath for the following reasons:

   a) Firstly, the surface area during oxygen blowing is far from flat. The total interface area between the slag and metal is enormous in comparison with the geometric circular area determined by the ladle radius. Thus, the reaction area of the surface is significantly bigger than the reaction site within the bath, resulting in a predominant value of β_{Surf}.

b) Secondly, as described by Kuwabara, Umezawa, Mori, and Watanabe (1988), the depth of reaction zone within the metal bath strongly decreases along with decreasing carbon content. Hence, the reaction of carbon with oxygen remains mainly on the surface and at the surface of the Ar bubbles. Since the carbon content after oxygen blowing is very low, this situation is definitely valid for the boil-off stage of the process.

The changes of the mass transfer coefficient can either be calculated based on the film theory, the penetration theory or the surface renewal theory. The mass transfer coefficient k_{Surf} is chosen to be 0.0015 $\mathrm{m\,s^{-1}}$. This is an average value from the analysis of several operation conditions based on the Penetration Theory. The mass transfer coefficient of carbon for the Ar bubble reaction site can be calculated as follows (T. Kitamura et al., 1996; S.-y. Kitamura, Yano, Harashima, & Tsutsumi, 1994; Wei & Zhu, 2002):

$$k_{Ar} = 2 \cdot \sqrt{\frac{D_C}{\pi \cdot \theta}} \tag{2.21}$$

$$\theta = \frac{d_{Ar}}{u_{Ar}} \tag{2.22}$$

$$u_{Ar} = 1.02 \cdot \sqrt{g \cdot \frac{d_{Ar}}{2}} \tag{2.23}$$

In these equations, D_C is the diffusion coefficient of carbon in liquid steel, θ is the contact time, d_{Ar} is the Ar bubble diameter and u_{Ar} is the rising velocity of the bubble.

Based on the above mentioned fact that the reaction area for the surface is far from flat, the present study introduces an effective reaction area, $A_{Surf-eff}$ and estimates this parameter as function of the blowing rate, Q_{O_2} (for the blowing stage) and as a function of the decarburization rate, D_C (for the boil-off stage):

$$A_{Surf-eff} = \begin{cases} A_{Surf} \cdot Q_{O_2} \cdot f_1 & if \;\; Q_{O_2} > 0 \\ A_{Surf} \cdot D_C \cdot f_2 & if \;\; Q_{O_2} = 0 \end{cases} \tag{2.24}$$

In these equations, f_1 and f_2 act as parameters for model adjustment. The surface area for the gas Ar bubbles can be estimated based on an estimation of the number of bubbles and their diameter (Díaz, Komarov, & Sano, 1997; Davies & Taylor,

1950):

$$A_{Ar} = d_{Ar}^2 \cdot \pi \cdot n_{Bubble} \tag{2.25}$$

$$n_{Ar} = \frac{6 \cdot Q_{Gas} \cdot H}{\pi \cdot d_{Ar}^3 \cdot u_{Ar}} \tag{2.26}$$

where H refers to the rising height (ladle height) and Q_{Gas} is the Ar flow rate. Finally, β can be calculated as follows:

$$\beta = \frac{\rho_{Steel}}{m_{Steel}} \cdot (k_{Surf} \cdot A_{Surf-eff} + k_{Ar} \cdot A_{Ar}) \tag{2.27}$$

2.3.5 Temperature Considerations

All the sub-models described so far determine changes to elements within the metal and slag phase. In the same way, the balance of the metal bath temperature is another key factor. A holistic metal bath temperature approach considers cyclic temperature losses (e.g. due to convection and radiation), event specific losses (e.g. due to stirring, oxygen injection jet or material additions) and temperature gains from the reactions with oxygen.

1. **Temperature Balance Block** (Sub-model VIII)
   The overall ΔT of a calculation step can be formulated as expressed by the following equations:

$$\Delta T_{Tot} = \Delta T_{Ladle} + \Delta T_{Process} + \Delta T_{Additions} \tag{2.28}$$

$$\Delta T_{Ladle} = \Delta T_{Wall} + \Delta T_{Bottom} + \Delta T_{Radiation} \tag{2.29}$$

$$\Delta T_{Process} = \Delta T_{Stirring} + \Delta T_{O_2-Jet} + \Delta T_{Reactions} \tag{2.30}$$

   Single calculation procedures of Equation (2.29) are according to (Çamdali & Tunç, 2006; Tian, Mao, & Wang, 2008; Gupta & Chandra, 2004). The determination of the temperature gains by oxidation is based on the following equation, where thermodynamic data like enthalpy change ΔH_i or the specific heat capacity c_p are extracted from relevant literature (e.g. Wei & Zhu, 2002):

$$\Delta T_{Reactions} = \sum_i \frac{\Delta m_i \cdot \Delta H_i}{m_{metal} \cdot c_p} \tag{2.31}$$

In this expression, the variable m_{metal} refers to the total mass of the metal bath. As far as Equation (2.28) considers a lot of process data and ladle data, it is often not useful for offline simulation.

For the present thesis, the complete calculation procedure for the temperature ladle loss explained in Equation (2.29) is replaced by a simple parameter. The adjustment parameter serves as input parameter and specifies exactly the average ladle loss in $\mathrm{K\,s^{-1}}$. This approach is used in the thesis for ladle-independent simulation of the process.

2.3.6 Sub-model Assembling

Using the above described model blocks (sub-models), the entire model procedure can be formulated as illustrated in Figure 2.1. At this point, the described model assembly uses some assumptions and simplifications. Undoubtedly, it is based on fundamental chemistry and physics. Still, by introducing more and more fundamental-based model blocks the complexity increases. Such an increase of complexity leads consequently to a higher number of necessary model parameters. Thus the model uses fundamental physics and chemical laws as the basis, accompanied with particular empiricism to simplify specific parts of the model.

In terms of the computation flow, the assembled model can be described as follows: at the beginning of the model, the initial conditions by the means of metal temperature, metal chemistry and slag chemistry are gathered. Based on these current conditions, the arguments for a calculation step are prepared. The arguments include the current process data (e.g. oxygen blowing rate, stirring rate, vacuum pressure, etc.), the chemistry and temperature. Importantly, the delta-time Δt of the simulation step must be known (e.g. for some real-time conditions a Δt of two or four seconds is sufficient). Before running the model, the adjustment parameters will be attached to the arguments. Next, this package of input data runs through the above described sub-models. At the end, a dedicated update method applies all the changes in terms of ΔT, Δm_i and Δm_j to the current conditions. Finally, the model is running the next cycle using the updated conditions and new available process data (Kleimt et al., 2006; Mayer et al., 2017).

3 Mathematical Problem Statement

As basis for any investigation on the outcome of the model and how it can be optimized, the model itself must be transformed into mathematical terms. Within the following chapter, the problem was separated into descriptive parts each optimization problem consists of: (1) description of used constants, (2) input parameters, (3) variables, (4) the objective function and (5) all necessary constraints. In order to determine the constants of the model, process data of heats in operation were collected from a customer. The samples illustrate the accuracy of the model in the field and consequently the acceptance of the used parameters for the research setting. For the deduction of the mathematical problem statement, the existing model is examined. Finally, the transformation of the existing model into the corresponding mathematical terms leads to a comprehensive description of the optimization problem.

3.1 Model Parameter Evaluation

The model, described on a more physical and theoretical basis, implements a set of adjustable parameters. As a matter of fact, every equipment and every operation in the field is different. Besides, the physics on which the model is based on remain the same. Thus, the model incorporates some reasonable parameters to adjust the calculation. Accordingly, the results of the model can be brought into the necessary acceptable range.

In order to provide a set of parameters for the further research, real process data from heats at an operating steel plant in South Korea were taken. During the on-site installation and commissioning of the model, metallurgists and modeling experts adjusted the model to calculate proper results. For the purpose of demonstration, twelve data sets of real produced heats were granted from the customer in South Korea. The process

#	Steel Grade	Steel, kg	Slag, kg	Temp., °C	C	Mn	Cr
1	S316L	98000	100	1625	0.360	1.22	15.77
2	F51	100900	50	1585	0.647	1.42	22.23
3	S316L	114800	100	1632	0.290	1.13	16.43
4	S316L	99200	100	1557	0.330	1.33	16.13
5	S316L	98700	100	1622	0.330	1.29	16.94
6	S304L	105000	200	1631	0.466	1.34	18.11
7	S304L	104000	100	1592	0.540	1.00	18.20
8	S316LP	107000	100	1595	0.590	1.15	17.10
9	S316LP	102000	100	1617	0.480	1.26	17.05
10	S304L	101500	500	1590	0.701	1.26	18.16
11	S304L	100400	200	1590	0.540	1.18	17.93
12	S316L	106000	500	1632	0.268	1.11	16.19

Table 3.1: Exemplary process data of VOD-treated heats from the field

data (taken during the adjustment phase of the model) show different heats and steel grades and are listed in Table 3.1. In detail, the data consist of four different steel grades: S304L, S316L, S316LP and FS51. All these steel grades are stainless steels. Within the steel grade type identifiers, t he post-fix "L" refers to the low-carbon version of the steel grade type. The grade 304 is the most popular stainless steel grade also known as the typical "18/8" as the make-up of the grade is 18% chromium together with around 8% of nickel. Second important steel grade of this type is the 316 standard molybdenum-bearing grade. The higher concentration of molybdenum gives the 316 grade better corrosion resistance compared to the 304. The F51 is a duplex stainless steel with a higher concentration of chromium (up to 23%) but less nickel concentration (between 4 and 6%) (AZoM, 2001). The steel grade mix was chosen to illustrate the capability of the model throughout various conditions. In detail, Table 3.1 shows different initial conditions of the samples in terms of steel and slag weight, temperature and chemical composition.

The evaluation procedure was carried out by comparing the measured carbon, chromium, manganese and temperature values to their calculated counterparts from the model installed. The command line interface of the developed model (program modelcli.exe) has the option to replay process data log files and simulate the production. The results of the simulation are the exact same values as the model predicted in real-time. In the same way, all granted data logs for the heats were simulated with the same set of parameters. The results shown in Figure 3.1 and 3.2 compare the measured values of carbon, chromium, manganese and temperature to the values calculated by the model. Referring to the modeling background (see Section 2.2.1), the prediction of the carbon

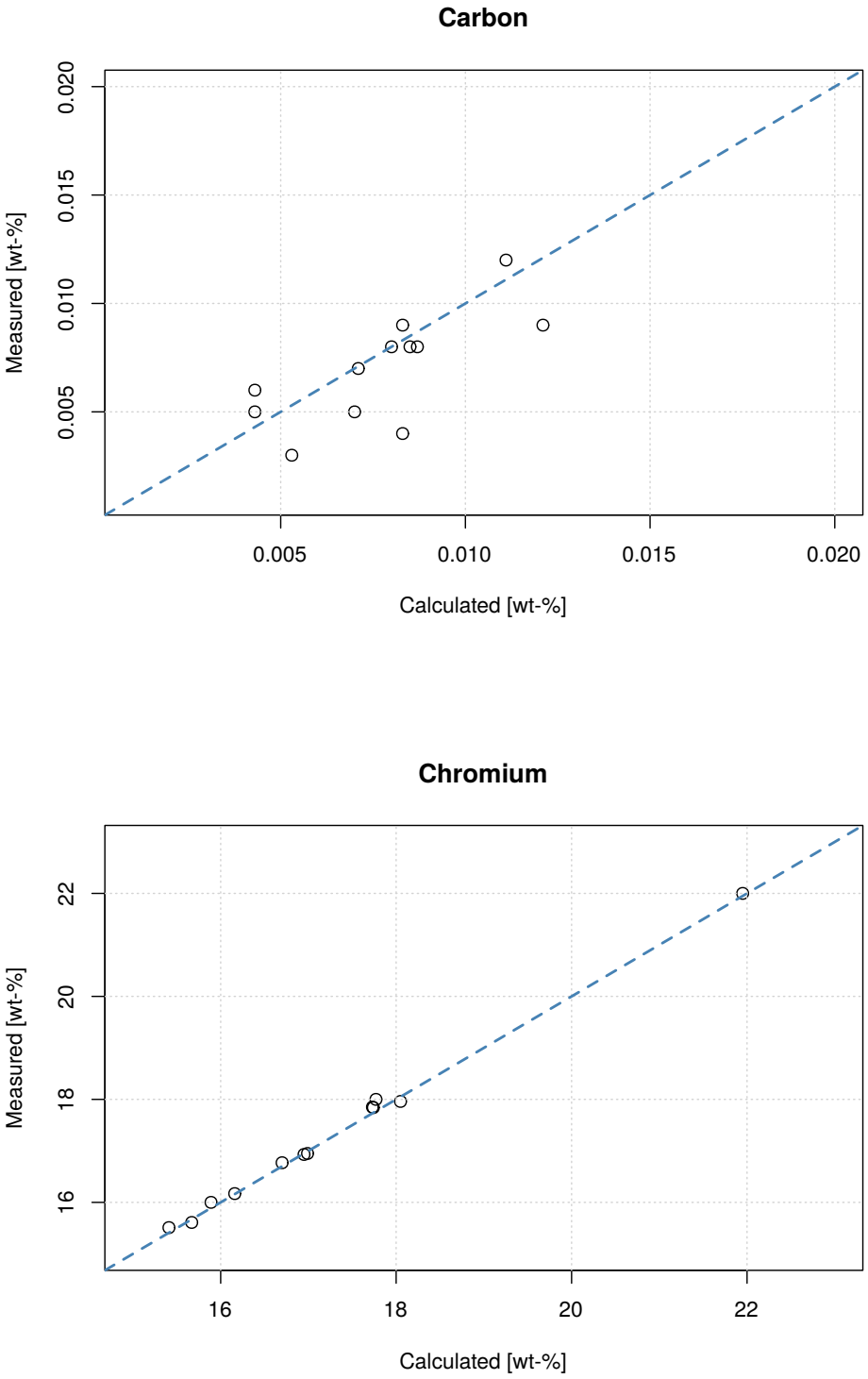

Figure 3.1: Measured values compared to model results in the field (C and Cr)

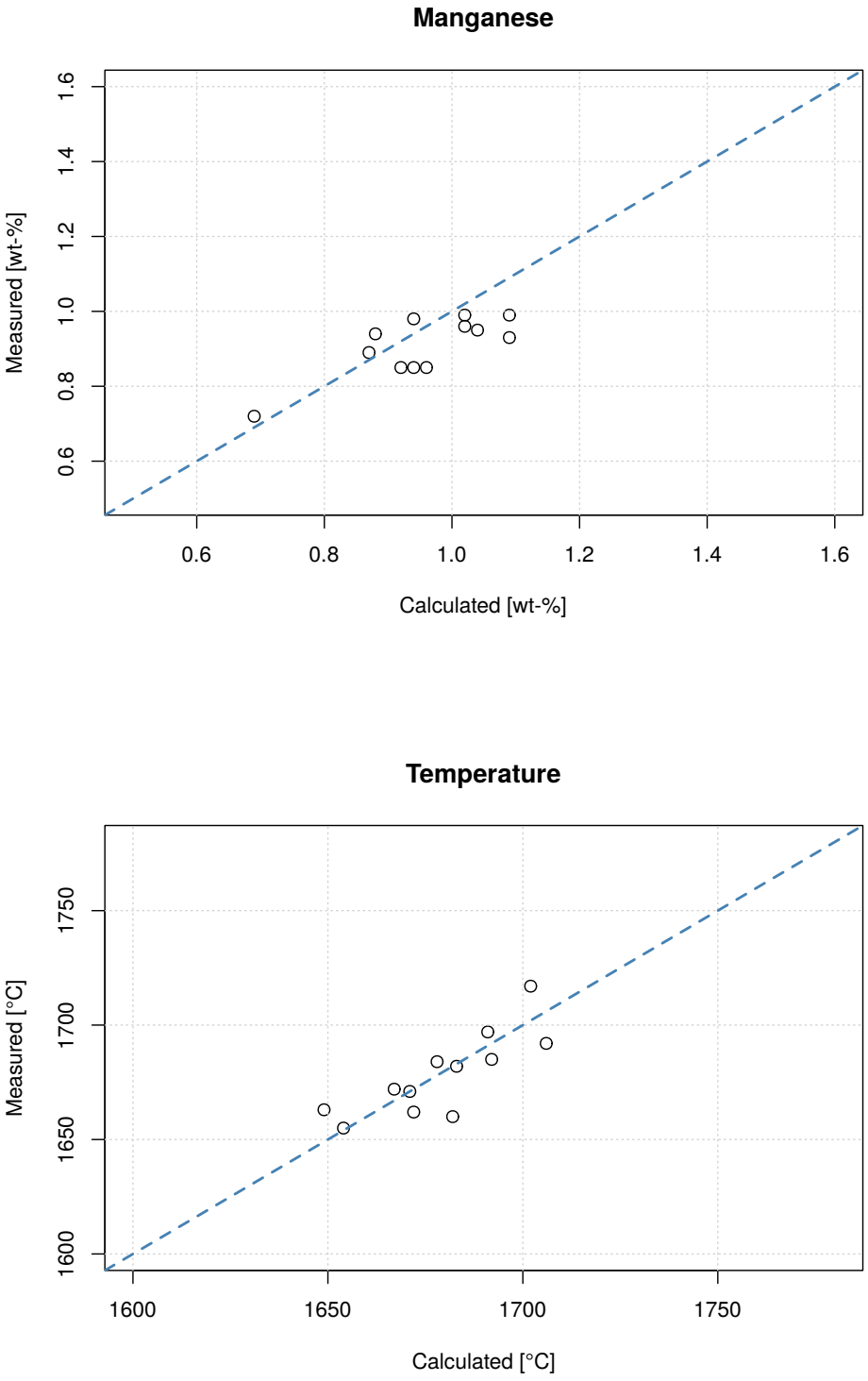

Figure 3.2: Measured values compared to model results in the field (Mn and temperature)

content together with a stable temperature is critical. Therefore, customers accept a certain level of standard deviation together with a given mean error. The VOD process of the sample heats achieved an obviously low amount of carbon. At the customer, of whom the samples were taken from, the model has been accepted with a standard deviation of 0.0035 with a mean error at 0.0005. Correspondingly, the set of parameters used to produce these results are used as the constants for the further research setting. These parameters are finally listed with name, value and unit in Table 3.2.

3.2 Mathematical Definition of the Optimization Problem

The mathematical definitions and statements in the following section are used to understand and reproduce the problem. As already stated in the introduction of this chapter, the definition of the optimization problem is subdivided into parts. Each part, from constants to constraints, is described in a dedicated sub-section.

3.2.1 Constants

Constants are coefficients which remain the same throughout the whole model calculation procedure. In other words, for each execution of the model as well as in each computation step, these coefficients have the same values and therefore remain constant. The constant coefficients of the present research setting are divided into two groups:

1. Physical and chemical constants: Even though physical constants can be determined and looked-up from the literature, the specific constants used in the calculations, are listed in Table 3.3. Constants of each element such as enthalpy of reaction ΔH_r^{Θ} and the stoichiometric factor ν used in the model implementation are listed in Table 3.4. The interactivity coefficients of elements, used for activity calculations are shown in Table 3.5.

2. The set of parameters based on the demonstration of the previous section: the constants of the model were examined with the simulation study described in the previous section and are listed in Table 3.2.

Description	Parameter	Value	Unit
Oxygen Yield	η_O	0.8	-
Oxygen Dissolution	c_O	0.03	-
Pressure Offset	p_{off}	10	-
Average Temperature Loss	T_{loss}	0.5	K
Vacuum Temperature Loss	T_{loss-p}	0.3	K
Vacuum Temperature Pressure Limit	p_{limit}	800	mbar
Ratio C	R_{C}	0.72	-
Ratio Cr	R_{Cr}	0.17	-
Ratio Mn	R_{Mn}	0.10	-
Ratio Fe	R_{Fe}	0.01	-

Table 3.2: Validated and accepted set of model-parameters in the field

Description	Constant	Value	Unit
Equilibrium Calculation Constant A	$\mathrm{KA_C}$	1168	-
Equilibrium Calculation Constant A	$\mathrm{KA_{Cr}}$	44040	-
Equilibrium Calculation Constant B	$\mathrm{KB_C}$	2.07	-
Equilibrium Calculation Constant B	$\mathrm{KB_{Cr}}$	-19.42	-
Heat Capacity of Steel	CP	850	-
Cooling Ratio of Oxygen Flow	$\mathrm{C_1}$	-1314.68	-

Table 3.3: General physical constants

Element	v	ΔH
C	0.932	8280000
Si	0.798	33768000
Mn	0.204	7416000
Cr	0.323	10872000
Al	0.623	31104000
Ti	0.468	11700000
Fe	0.201	4680000

Table 3.4: Stoichiometric factors ν and enthalpy coefficients ΔH

$e_C^C = \frac{358}{T}$	$e_C^{Cr} = \frac{-54}{T} + 0.006$	$e_C^{Ni} = 0.008$	$e_C^O = -0.34$
$e_{Cr}^C = \frac{-234}{T} + 0.012$	$e_{Cr}^{Cr} = 0$	$e_{Cr}^{Ni} = -0.009$	$e_{Cr}^O = 0$
T_{K} refers to the current temperature in Kelvin			

Table 3.5: Interacting coefficients for carbon and chromium

Besides the constant coefficients defined, in fact the model needs chemical elements and compounds. Elements in the metal bath and compounds in the slag area. In order to use the chemical elements and compounds in various mathematical formulations, the following definitions were made for

$$\begin{aligned} \text{elements} \quad & E := \{\mathrm{C}, \mathrm{Si}, \mathrm{Mn}, \mathrm{P}, \mathrm{S}, \mathrm{Cr}, \mathrm{Ni}, \mathrm{Mo}, \mathrm{Cu}, \mathrm{Ti}, \mathrm{Al}\} \\ \text{compounds} \quad & C := \{\mathrm{CaO}, \mathrm{SiO_2}, \mathrm{MgO}, \mathrm{Al_2O_3}, \mathrm{FeO}, \mathrm{MnO}, \mathrm{Cr_2O_3}\} \\ \text{summarized to} & \\ \text{all symbols} \quad & A := E \cup C \end{aligned} \tag{3.1}$$

3.2.2 Input Parameters

The input parameters, also termed as start conditions of the calculation cycle, are typically defined by the steel grade used. The initial conditions are process parameters which cannot be changed by any optimization algorithm. The input parameters used, were categorized into the following three major parts:

1. Start conditions of metal bath: On the one hand, the input parameters for the metal bath contain process related information such as start temperature T_{start} [°C] and metal bath weight m_{metal} [kg]. On the other hand, the metal bath conditions contain the initial values for the chemical composition of the metal bath in weight percent w [%].

2. Start conditions of slag area: Similarly to the metal bath, the slag area consists also of the process related information of the total mass m_{slag} [kg] and the initial values of the slag chemistry also in weight percent w [%].

3. Input parameters towards the required target solution: Clearly, the most obvious target setting is the target concentration of carbon after the decarburization process. Hence, the parameter C_{target} [%] was introduced to lead the model to the required carbon content. Further parameters are used to frame the model within the capabilities of the process and the equipment:

   - the minimum possible flow of oxygen O_{min} [$\mathrm{m^3\,h^{-1}}$],
   - the maximum possible flow of oxygen O_{max} [$\mathrm{m^3\,h^{-1}}$],

- the maximum system pressure during the main-decarburization p_{main} [mbar],
- minimum possible system pressure $p_{\min}$ [mbar],
- maximum time allowed $t_{\max}$ [s].

3.2.3 Variables

From the domain-specific point of view, the process is carried out by a programmable logic controller (PLC) controlling the equipment using predefined set-points. The definition is usually done in advance of the process and often named oxygen-blowing-pattern. Pattern, because of the inherent relation of each set-point to time. Such a pattern can be directly translated to the set of variables for the optimization problem. Importantly, the connection between the three variables: system pressure, oxygen rate and stirring gas rate; and their relation to time is critical. Moreover, based on the capabilities of the process and the equipment, the variables in the target oxygen-blowing-pattern are limited to a maximum of 8 different levels. Speaking differently, 8 allowed steps times 3 variables would result in 24 different variables only. On the contrary, the offline simulation tool evaluates the condition of the heat in terms of temperature, metal- and slag chemistry for every time-interval Δt. As a simplification, to use the existing directly, each process parameter results in a single variable per Δt. Furthermore, to comprise another simplification: Δt is set to be 1 [s] to spare the time-correlated term in some mathematical expressions. As a result, the variables of the optimization model are defined as:

1. system pressure [mbar]:

   $$P_t \quad \text{with} \quad t = 1, \ldots, t_{\max}$$

2. oxygen rate [$\text{m}^3\,\text{h}^{-1}$]:

   $$O_t \quad \text{with} \quad t = 1, \ldots, t_{\max}$$

3. stirring gas rate [$\text{L}\,\text{min}^{-1}$]:

   $$S_t \quad \text{with} \quad t = 1, \ldots, t_{\max}$$

In order to ensure the mentioned maximum of 8 different levels per variable, an additional parameter for each variable was necessary. Speaking in terms of a staircase function, the maximum allowed steps are 8 over the entire process. This can be expressed by a function (δ), which is used to determine two conditions. Consequently, the additional parameter for the system pressure variable is introduced as:

$$\delta_t^P := \begin{cases} 0 & \dots \quad P_{t-1} = P_t \\ 1 & \dots \quad P_{t-1} \neq P_t \end{cases}$$

$$\sum_{t=0}^{t_{\max}} \delta_t^P \leq 8 \quad \text{with} \quad P_0 = 0$$

In the present thesis, the function δ_t^P is 0 whenever the previous variable is equal to the current variable and 1 if they are different. To summarize, the defined function is 1 whenever there is a step. Hence, the sum of the function is used to limit the steps to allowed number. In addition, this approach is also applied for the oxygen rate:

$$\delta_t^O := \begin{cases} 0 & \dots \quad O_{t-1} = O_t \\ 1 & \dots \quad O_{t-1} \neq O_t \end{cases}$$

$$\sum_{t=0}^{t_{\max}} \delta_t^P \leq 8 \quad \text{with} \quad P_0 = 0$$

as well as for the stirring gas rate:

$$\delta_t^S := \begin{cases} 0 & \dots \quad S_{t-1} = S_t \\ 1 & \dots \quad S_{t-1} \neq S_t \end{cases}$$

$$\sum_{t=0}^{t_{max}} \delta_t^S \leq 8 \quad \text{with} \quad S_0 = 0$$

Referring to the optimization problem, the introduced δ-functions above are also used as constraints to the objective function by limiting their sum to the allowed number of 8.

As mentioned above, to predict the conditions of a heat during the VOD process, the model evaluates the temperature and chemical composition of metal bath and slag area. The result of the calculations lead to updated conditions of the heat and serve as input for the next calculation cycle. In other words, similarly to the variables itself, these conditions

are in relation to time: a calculated value for each time-interval Δt. On the one hand, the temperature is defined as T_t [°C]. On the other hand, the chemical composition of the metal bath and the slag area are defined as:

$$\begin{aligned} \text{mass [kg]} \quad & m_{x,t} \quad \text{with} \quad x \in A \\ \text{total steel mass [kg]} \quad & m_{metal,t} = \sum_{x \in E} m_{x,t} \\ \text{total slag mass [kg]} \quad & m_{slag,t} = \sum_{y \in C} m_{y,t} \end{aligned}$$

from this follows that:

$$\begin{aligned} \text{weight percent [wt-\%]} \quad & w_{x,t} = \frac{m_{x,t}}{m_{metal,t}} \cdot 100 \quad \text{with} \quad x \in E \\ \text{weight percent [wt-\%]} \quad & w_{y,t} = \frac{m_{y,t}}{m_{slag,t}} \cdot 100 \quad \text{with} \quad y \in C \end{aligned}$$

The concrete calculation of $m_{x,t}$, $m_{y,t}$ and T_t for each time-interval together with the derivation of the objective function will be explained in the subsequent sub-section.

3.2.4 Objective Function

As described in the metallurgical background section, the VOD process in general aims to oxidize carbon in order to reach lowest carbon contents in the final steel chemistry. Undoubtedly, a certain carbon level C_{target} has to be reached at all costs. In contrast to the necessity of reaching the carbon content, the oxidation of side elements during the process can be minimized. By far, the most expensive side effect is the oxidation of chromium. Due to the presence of high chromium contents in certain steel grades, the oxidation of chromium is somehow inevitable and happens due to thermodynamics and physics. The expense comes with the costs of required raw-material to reduce the chromium-oxide (Cr_2O_3) formed in the slag area. As a consequence, the objective function of the model must minimize the formation of chromium-oxide in the slag area and has been defined as:

$$\min \sum_{t=t_{\mathrm{start}}}^{t_{\max}} (O_t \cdot \eta_O \cdot R_{\mathrm{Cr}} + k_t) \tag{3.2}$$

Equation 3.2 can be understood as the minimization of the amount of oxygen [m^3], which react with chromium to form chromium-oxide during decarburization. According to the existing model, the equation considers the unavoidable amount of chromium oxidation, expressed as ratio R_{Cr}. The dynamic amount of oxygen, which additionally accounts for chromium is due to kinetics in decarburization.

The kinetic mass transfer approach is highly influenced by the system pressure and considers the stirring conditions additionally. According to the fundamental description of the model from Equation (3.3) to (3.7), the time-related parameter k_t is deduced as:

$$k_t = \max\left\{\left(O_t \cdot \eta_O \cdot R_{\mathrm{C}} - d\mathrm{C}_{\mathrm{kin},t} \cdot \nu_{\mathrm{C}}\right), 0\right\} \tag{3.3}$$

The max function for k_t is mandatory in order to neglect negative values whenever the kinetic rate is higher than the stoichiometric rate:

$$d\mathrm{C}_{\mathrm{kin},t} = \max\left\{\left(\beta_t \cdot (w_{\mathrm{C},t} - eqm_{\mathrm{C},t}) \cdot \frac{m_{\mathrm{metal},t}}{100}\right), 0\right\} \tag{3.4}$$

Also for Equation (3.4), the max function is required to make sure the kinetic rate cannot get negative in case the carbon in equilibrium is higher as the current carbon content.

In order to overcome the complexity described in β-model section of the theoretical background, the optimization problem was simplified. With this intention, two fixed values for β were defined as tuning parameters. The first one is used during oxygen blowing, whereas the second one is used for boil-off:

$$\beta_t := \begin{cases} \beta_1 & \dots \quad O_t > 0 \\ \beta_2 & \dots \quad O_t = 0 \end{cases} \tag{3.5}$$

As described in the background section, the driving force for the kinetic decarburization rate is the carbon content in equilibrium condition. Accordingly, the mathematical formulation is defined as:

$$eqm_{\mathrm{C},t} = F_{\mathrm{CO},t} \cdot p_{\mathrm{CO},t} \tag{3.6}$$

The following paragraph describes the derivation of the first part, which is $F_{\mathrm{CO},t}$, of the carbon equilibrium conduction:

$$F_{\mathrm{CO},t} = \frac{a_{\mathrm{Cr},t}^{\frac{2}{3}} \cdot K_{\mathrm{Cr}}}{f_{\mathrm{C},t} \cdot K_{\mathrm{C}} \cdot \sqrt[3]{a_{\mathrm{Cr_2O_3},t}}} \tag{3.7}$$

The calculations of the equilibrium constants were deduced from the equations 2.19 and 2.20 from the model description section:

$$\begin{aligned} \log K_{\mathrm{C}} &= \frac{\mathrm{KA_C}}{T_t} + \mathrm{KB_C} \\ K_{\mathrm{C}} &= 10^{\log K_{\mathrm{C}}} \\ \log K_{\mathrm{Cr}} &= \frac{\mathrm{KA_{Cr}}}{T_t} + \mathrm{KB_{Cr}} \\ K_{\mathrm{Cr}} &= 10^{\log K_{\mathrm{Cr}}} \end{aligned} \tag{3.8}$$

The current metal bath temperature plays another important role for the equilibrium calculation. As carried out above, the calculation steps are conducted from the corresponding references in the theoretical background section (Equations 2.29 and 2.30). For the optimization problem, the temperature balance is defined as follows for each time-interval:

$$\begin{aligned} T_t &= T_{t-1} + \Delta T_t \\ \Delta T_t &= \frac{-T_{loss} \cdot \Delta t}{60} - \frac{T_{loss-p} \cdot \Delta t}{60} \cdot \delta_t^{p-limit} \\ &\quad + \sum_{x \in E} \frac{\Delta m_{x,t} \cdot \Delta H_x}{m_{metal,t-1} \cdot \mathrm{CP}} \\ &\quad - \frac{\mathrm{C_1} \cdot O_t \cdot (T_t - 30)}{m_{metal,t-1} \cdot \mathrm{CP}} \end{aligned} \tag{3.9}$$

The additional temperature loss, which accounts during low system pressure, is formulated by defining another δ function. It is defined to be 1 whenever the current system pressure is below the given limit, otherwise 0. The limit is taken from the constants. Consequently, the second term of Equation (3.9) multiplied with the $\delta_t^{p-limit}$ function is accounted according to the pressure conditions:

$$\delta_t^{\mathrm{p-limit}} := \begin{cases} 1 & \dots \quad P_t \leq p_{limit} \\ 0 & \dots \quad P_t > p_{limit} \end{cases} \tag{3.10}$$

Another important part of calculating the carbon in equilibrium condition are the activity and activity coefficients of elements and compounds. These coefficients are implemented to be executed at first of each calculation cycle of the model and can be expressed as:

$$\begin{aligned} \log f_{x,t} &= \sum_{k \in E} e^k_{x,t} \cdot w_{k,t} + e2^k_x \cdot w^2_{k,t} \\ f_{x,t} &= 10^{\log f_x} \\ a_{x,t} &= f_{x,t} \cdot w_{x,t} \end{aligned} \tag{3.11}$$

given that $\forall x \in E$ and $t = 1, \ldots, t_{\max}$

As pointed out in the modeling background section, the activities of compounds in the slag area are often based on empirical calculations. The present mathematical problem statement simplified the activity calculation by dismissing the Gibbs minimization problem. Hence, the only used slag compound activity is the one of chromium-oxide. Referring to the chromium-oxide activity calculation of the related work (see Section (2.12)), the formulation is carried out as:

$$\begin{aligned} n_{y,t} &= \frac{1000 \cdot m_{y,t}}{\mathrm{M}_y} \\ n_{tot,t} &= \sum_{y \in C} n_{y,t} \\ X_{y,t} &= \frac{n_{y,t}}{n_{tot,t}} \\ a_{\mathrm{Cr_2O_3},t} &= 2.9505 \cdot U_t^{0.6899} \cdot X^{V_t}_{\mathrm{Cr_2O_3},t} \end{aligned} \tag{3.12}$$

The calculation of U_t and V_t is extracted and stated in the following:

$$\begin{aligned} U_t &= \frac{X_{\mathrm{CaO},t}}{X_{\mathrm{SiO_2},t}} \\ V_t &= -0.4249 \cdot U_t^4 + 1.7879 \cdot U_t^3 - 2.6886 \cdot U_t^2 + 1.5492 \cdot U_t + 1.3126 \end{aligned} \tag{3.13}$$

Taking a step back to the carbon equilibrium calculation of Equation (3.6), the partial pressure of the system $p_{\mathrm{CO},t}$ is the second required term. The calculation of this term is realized as follows:

$$p_{\mathrm{CO},t} = (P_t + p_{add,t}) \cdot \frac{p_{corr,t}}{1000} \tag{3.14}$$

$$p_{add,t} = p_{off} \cdot -P_t^{2 \cdot p_{off}} \tag{3.15}$$

$$
\begin{aligned}
p_{corr,t} &:= \begin{cases} 1 & \dots \quad d\mathrm{C}_{t-1} \leq 0 \\ \frac{r_{\mathrm{CO}}}{r_{\mathrm{CO}}+S_t} & \dots \quad \text{otherwise} \end{cases} \\
r_{\mathrm{CO}} &= d\mathrm{C}_{t-1} \cdot \frac{22.4}{12000} \cdot m_{\mathrm{metal},t-1} \\
&\text{with} \quad d\mathrm{C}_0 = 0
\end{aligned}
\tag{3.16}
$$

Another key part is the parameter t_{start} used in the objective function. Since the model comprises simplifications and the influence on the final result is significantly low, the decarburization will not start until the complete oxidation of Al, Ti and Si. The algorithm can be mathematically expressed as:

$$
\begin{aligned}
\delta_t^{\mathrm{start}} &:= \begin{cases} 1 & \dots \quad (m_{\mathrm{Al},t} - \Delta m_{\mathrm{Al},t} + m_{\mathrm{Ti},t} - \Delta m_{\mathrm{Ti},t} + m_{\mathrm{Si},t} - \Delta m_{\mathrm{Si},t}) > 0 \\ 0 & \dots \quad \text{otherwise} \end{cases} \\
t_{\mathrm{start}} &= \sum_{t=0}^{t_{\max}} \delta_t^{\mathrm{start}}
\end{aligned}
\tag{3.17}
$$

By doing so, the $\delta_t^{\mathrm{start}}$ function is 1 until all the priority elements are oxidized. At the same time, this implies that the model oxidizes these priority elements at the beginning. Moreover, the model sequentially oxidizes these elements in the following order: Al, Ti and Si. In other words, the oxidation of the priority elements causes another fact to be described: the decrease of $m_{x,t}$ over time. This decrease of the masses of elements $m_{x,i}$ happens due to the oxidation per time-interval. This process can be mathematically formulated as:

$$
\begin{aligned}
m_{x,t} &= m_{x,t-1} + \Delta m_{x,t} \\
\Delta m_{x,t} &= \frac{O_{x,t}}{\nu_x} \quad \text{with} \quad x \in E \\
\Delta m_{y,t} &= \Delta m_{x,t} \cdot \nu_y \quad \text{with} \quad x \in E \wedge y \in C
\end{aligned}
\tag{3.18}
$$

The variable $O_{x,t}$ will be determined during the calculation sequence. Firstly, the amount of oxygen is going to be reduced by multiplying with η_O, which considers the overall oxygen yield. Secondly, it depends on the oxidation of the mentioned priority elements. For these, the remaining oxygen amount after yield is used directly. Thirdly, for the main decarburization phase, the remaining amount of oxygen will be distributed according to the ratios R_{C}, R_{Cr}, R_{Mn} and R_{Fe}. However, a demonstration of the complete calculation cycle with exemplary is carried out and explained in the successive chapter.

As the last step of this section and in order to execute the model, the following expressions indicate the take-over of the input parameters to the start conditions of the model:

$$\begin{aligned} T_0 &= T_{start} \\ m_{x,0} &= \frac{w_x}{100} \cdot m_{metal} \quad \forall x \in E \\ m_{y,0} &= \frac{w_y}{100} \cdot m_{slag} \quad \forall y \in C \\ m_{metal,0} &= m_{metal} \\ m_{slag,0} &= m_{slag} \end{aligned} \tag{3.19}$$

3.2.5 Constraints

To carry out the VOD process, metallurgists rely on many boundary conditions. Some of them are based on the capabilities of the equipment itself. For example, the pressure system (mechanical pumps or steam pump system) controls the pressure level which can be reached during the process. Other conditions come from the process. For example, during the main decarburization process (the phase where most of the carbon reacts with oxygen) the high amount of off-gas in the tank makes it hard to hold a certain pressure level. In order to consider these boundary conditions and the general capability of the decarburization process, the optimization model must adhere the following constraints:

$$\begin{aligned} w_{\mathrm{C},t_{\max}} &\leq \mathrm{C}_{target} \\ O_t &\leq O_{\max} \cdot B_t \quad \forall t = 1, \ldots, t_{\max} \\ O_t &\geq O_{\min} \cdot B_t \quad \forall t = 1, \ldots, t_{\max} \\ P_t &\geq P_{\min} \quad \forall t = 1, \ldots, t_{\max} \end{aligned} \tag{3.20}$$

Considering the boil-off phase at the end of the pattern, the oxygen blowing rate must be allowed to be zero. Thus, to ensure the oxygen blowing rate is either within the given range or zero, the auxiliary binary variable:

$$B_t \in \{0, 1\}$$

is defined, for which applies:

$$B_{t-1} \geq B_t \quad \forall t = 1, \ldots, t_{\max}$$

Besides the constraints identified in Equation (3.20), there exist more complex boundary conditions, which the optimization has to fulfill. At first, the beginning of the process by means of oxidizing the priority elements cannot be optimized due to equipment lifetime considerations. The combustion of Al, Ti and Si causes extreme turbulence which may harm equipment parts. Therefore, process engineers want to fix the oxidation at the beginning with 80% of the maximum allowed oxygen flow rate. This constraint is implemented with:

$$O_t = O_{\max} \cdot 0.8 \quad \forall t = 1, \ldots, t_{\text{start}} \tag{3.21}$$

In order to consider a certain system pressure level during the main decarburization phase, a pressure limit has been introduced. In advance, the determination of the main decarburization is conducted by:

$$\delta_t^{\text{main}} := \begin{cases} 1 & \ldots \quad d\text{C}_{\text{kin},t} > d\text{C}_{\text{sto},t} \wedge w_{\text{C},t} > 0.15 \\ 0 & \ldots \quad \text{otherwise} \end{cases} \tag{3.22}$$

For this expression, the δ_t^{main} function is 1 until the kinetic decarburization rate is smaller than the stoichiometric decarburization rate. Due to the decarburization start temperature, as included in the calculations of $F_{\text{CO},t}$, the kinetic rate can be smaller than the stoichiometric counterpart at the beginning. To overcome this, a lower limit of carbon concentration is introduced. The value of 0.15 assumes that the critical carbon content must be below this value. Firstly, the definition of the stoichiometric decarburization rate is required:

$$d\text{C}_{\text{sto},t} = \frac{O_t \cdot \eta_O \cdot R_{\text{C}}}{\nu_{\text{C}}} \tag{3.23}$$

Secondly and based on these equations, the critical point is defined as follows:

$$t_{crit} = \sum_{t=1}^{t_{\max}} \delta_t^{\text{main}} \tag{3.24}$$

Consequently, the system pressure constraint during the main decarburization phase can be defined as:

$$P_t \geq p_{\text{main}} \quad \forall t = 1, \ldots, t_{crit} \tag{3.25}$$

For the sake of completion, constraints which were already identified during the definition of the variables or the objective function are defined once again as necessary constraints for the model:

$$\sum_{t=1}^{t_{max}} \delta_t^O \leq 8 \tag{3.26}$$

Since the δ function evaluate to 1 whenever the current oxygen rate is different to the previous one, the sum of all detected differences of the function can be used to define the constraint. Equally, the constraints are defined for the system pressure and the stirring gas variables:

$$\sum_{t=1}^{t_{max}} \delta_t^P \leq 8 \tag{3.27}$$

$$\sum_{t=1}^{t_{max}} \delta_t^S \leq 8 \tag{3.28}$$

In order to avoid that the a possible optimization algorithm uses less amount of oxygen than minimum required based on stoichiometric physics, the following constraint was added:

$$\begin{aligned} \sum_{t=1}^{t_{max}} O_t \cdot \eta_{\mathrm{O}} \geq\ & (m_{\mathrm{Al},0} \cdot \nu_{\mathrm{Al}} + m_{\mathrm{Ti},0} \cdot \nu_{\mathrm{Ti}} + m_{\mathrm{Si},0} \cdot \nu_{\mathrm{Si}}) \\ & + \left(m_{\mathrm{C},0} - \frac{\mathrm{C}_{\mathrm{target}}}{100} \cdot m_{\mathrm{metal},0} \right) \cdot \nu_{\mathrm{C}} \end{aligned} \tag{3.29}$$

The equation basically states, that the sum of all oxygen variables in $\mathrm{m}^3\,\mathrm{s}^{-1}$ multiplied with the given η_{O} must be greater or at least equal to the required oxygen mass to oxide the priority elements plus the necessary oxygen for the carbon oxidation until the specified target carbon content C_{target}.

4 Variable Study

Based on theoretical background, the previous chapter dealt with the examination of the existing VOD process model. Moreover, the main part was the transformation of what the model does in real-time into a mathematical description of an optimization problem. As a result, all parts required, to rate or assess a solution are described in the previous chapter. As this can be seen as basis, the present chapter discusses the effect of variables on the model and finally on the objective function. By doing so, the first part of this chapter illustrates in detail how the result of the objective function is calculated. Therefore, an exemplary solution is defined from scratch to demonstrate the step-wise computation. Afterwards, the conduction of the result of the objective function can be seen as the calculation procedure for all given solutions. To remember, a solution is defined as the variables with concrete figures, which fulfills all constraints and leads to a deterministic result of the objective function. With this in mind, the last section of the present chapter compares different solutions with variable modifications. In detail, different solutions were compared by comparing the value of the objective function.

4.1 Illustrative Calculation Example Based on a Predefined Solution

In order to explain the determination of the model results, the following sub-section describes the calculation steps of the model in detail by using an illustrative example. Based on the constants, input parameters as well as the variable pattern described in the previous sections, the computation of each model block and calculation step will be explained in detail with concrete numbers. Therefore, randomly chosen variables are used as a possible solution for exemplary data. Using different words, the illustrative example shows the calculation cycle of the model with an arbitrary but feasible solution.

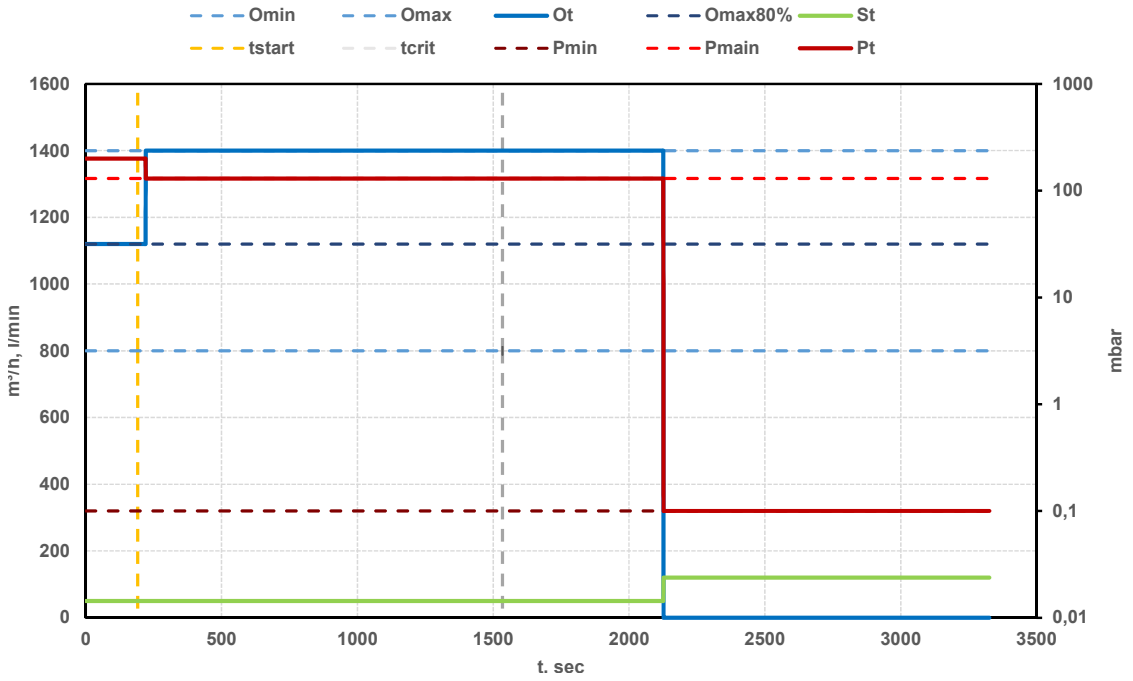

Figure 4.1: Example of a predefined feasible solution for given input parameters

The input parameters for the illustrative example are defined randomly, but describe a heat in the range of a typical 316L stainless steel grade. The VOD start temperature is defined to be 1590 °C. The initial mass for the metal bath is 110000 kg. At last, the metal bath composition at the beginning of the example is defined to be:
C = 0.400%, Si = 0.05%, Mn = 1.2%, P = 0.025%, S = 0.005%, Cr = 16.3%, Mo = 2.0%, Ni = 10.1%, Cu = 0.28%, Al = 0.005%;
Likewise, the initial slag mass is 100 kg and its composition is defined to be:
CaO = 45%, SiO_2 = 23%, MgO = 9%, Al_2O_3 = 11%, FeO = 5.5%, MnO = 2%, Cr_2O_3 = 4.5%;

Further objective and constraint related input parameters are:

$$\mathrm{C}_{\mathrm{target}} = 0.005\%$$
$$O_{\mathrm{min}} = 800\mathrm{m}^3$$
$$O_{\mathrm{max}} = 1400\mathrm{m}^3$$
$$p_{\mathrm{main}} = 130\mathrm{mbar}$$
$$p_{\mathrm{min}} = 0.1\mathrm{mbar}$$
$$t_{\mathrm{max}} = 5000\mathrm{s}$$

The feasible solution defined for the variables is shown in Figure 4.1. The solution leads to a certain value of the objective function and fulfills the requirements of the constraints by calculating each time-interval after another. Thus, the following sub-section illustrates this calculation in detail.

4.1.1 Step-wise Calculation of the Initial and an Arbitrary Time-step

The exact calculation routines and necessary preparation steps are described in the following. The explanation is separated into different model blocks executed in a sequential flow. The flow, as well as the model blocks were visualized in Figure 2.1 within the model description section. Therefore, the illustrative example uses cross references to refer to mentioned model blocks. In general, the model calculates the conditions based on the variables and conditions related to time. The model engine or executable deals with the time relation in the following manner: firstly, the model prepares the initial conditions; secondly, for each time-interval the model engine provides the process data which comes directly from the variables (oxygen blowing pattern). In the research setting, 1 second was defined as the time-interval to spare the time-related term in the mathematical formulations.

To summarize, the model simulation engine creates a bag of data based on the input parameters. These conditions together with the process data for the time-interval will be sent to the model library. The result from the model library updates these conditions. In the next step, the model library will be called with the updated conditions together with the next set of process data for the next time-interval. This process continues until the complete pattern shown in Figure 4.1 is calculated. The last updated conditions represent the final predicted state of the heat in terms of temperature, steel and slag chemistry. The pseudo-code snipped in Algorithm 4.1 shows the described flow of the existing process model.

For the sake of clarity, the calculated numbers during the following step-wise illustration are rounded to a reasonable number of decimal places. However, every calculation step is carried-out with a software tool, which calculates with the most precise numbers.

Initial Time-step

Based on Algorithm 4.1, the following explanation shows the results calculated for the

Algorithm 4.1 VOD model execution based on given input parameters and variables

```
1: create heat conditions from configuration file
2: read records (variables) from configuration file
3: for all records do
4:    conduct steel activity for heat
5:    conduct slag activity for heat
6:    oxidize priority elements Al, Ti and Si
7:    if all priority elements oxidized then
8:       calculate β
9:       calculate kinetic rate
10:      calculate stoichiometric rate
11:      if kinetic rate < stoichiometric rate then
12:         oxidize carbon kinetic amount
13:      else
14:         oxidize carbon stoichiometric amount
15:      end if
16:      oxidize left-over oxygen with Cr, Mn and Fe according to distribution
17:   end if
18:   calculate temperature balance
19:   conduct ladle temperature loss
20:   conduct vacuum temperature loss
21: end for
```

exemplary data with t = 1 and the time-interval Δt = 1. At first, the following expressions are used to illustrate the conditions at the start of the model execution for $t = 1$. The initial conditions were described in Equation (3.19) of the mathematical problem statement. These conditions, moreover the values, are taken over as start conditions from the input parameters:

$$
\begin{aligned}
T_0 &= 1590\ \text{°C} \\
m_{tot,0} &= 110000\ \text{kg} \\
O_1 &= 1120\ \text{m}^3\,\text{h}^{-1} \approx 0.311\ \text{m}^3\,\text{s}^{-1} \\
P_1 &= 200\ \text{mbar} \\
S_1 &= 50\ \text{L}\,\text{min}^{-1} \approx 0.00083\ \text{m}^3\,\text{s}^{-1}
\end{aligned}
$$

The first two blocks executed by the model are the fundamental steel- and slag activity blocks. The numerical calculation of the activity and activity coefficient of carbon and chromium using Equation (3.11) is calculated as described in the following equations. Importantly, all of them are using the temperature in K. Thus, the following transformation

is performed:

$$T = 1590 + 273.15\,\mathrm{K}$$

Afterwards, the steel- and slag activities are calculated as illustrated in the following for carbon:

$$\begin{aligned}
\log f_{\mathrm{C},1} &= \frac{358}{T} \cdot 0.4 + \left(\frac{-54}{T} + 0.006\right) \cdot 16.3 - 0.34 \cdot 0 + 0.008 \cdot 10.15 \\
f_{\mathrm{C},1} &= 10^{-0.2165} \\
a_{\mathrm{C},1} &= 0.607342 \cdot 0.4 \\
a_{\mathrm{C},1} &= 0.2429
\end{aligned}$$

Similarly, the chromium activity calculation for $t = 1$ is carried as follows:

$$\begin{aligned}
\log f_{\mathrm{Cr},1} &= \left(\frac{-234}{T} + 0.012\right) \cdot 0.4 + 0 \cdot 16.3 - 0.34 \cdot 0 - 0.009 \cdot 10.15 \\
f_{\mathrm{Cr},1} &= 10^{-0,1368} \\
a_{\mathrm{Cr},1} &= 0.729814 \cdot 16.3 \\
a_{\mathrm{Cr},1} &= 11.8960
\end{aligned}$$

Followed by the calculation of the carbon and chromium activities, the chromium-oxide slag activity needs to be evaluated. Thus, the terms explained with the Equations (3.12) and (3.13) are executed for $t = 1$. By doing so, the molar mass and molar fraction of all slag components are calculated. Representational for all slag components, the calculation for chromium-oxide is illustrated in the following expression:

$$\begin{aligned}
n_{\mathrm{Cr_2O_3},1} &= \frac{1000 \cdot 4.5}{151.9904} \\
X_{\mathrm{Cr_2O_3},1} &= \frac{29.6071}{1650.8352} \\
&\dots \\
X_{\mathrm{Cr_2O_3},1} &= 0.0179 \\
X_{\mathrm{CaO},1} &= 0.4861 \\
X_{\mathrm{SiO_2},1} &= 0.2319
\end{aligned}$$

Based on the preconditions of the compounds, the activity of the chromium-oxide is finally calculated as follows:

$$
\begin{aligned}
U_1 &= \frac{X_{\mathrm{CaO},1}}{X_{\mathrm{SiO_2},1}} \\
V_1 &= -0.4249 \cdot 2.0962^4 + 1.7879 \cdot 2.0962^3 - 2.6886 \cdot 2.0962^2 \\
&\quad + 1.5492 \cdot 2.0962 + 1.3126 \\
a_{\mathrm{Cr_2O_3},1} &= 2.9505 \cdot 2.0962^{0.6899} \cdot 0.01793^{1.0104} \\
a_{\mathrm{Cr_2O_3},1} &= 0.1153
\end{aligned}
$$

After calculating the thermodynamic basic conditions, the model oxidizes the priority elements in the order as described in the previous section, starting with aluminum. According to the Equation (3.18), the delta mass aluminum in the time-step $t = 1$, which will be oxidized can be computed with:

$$
\begin{aligned}
O_{\mathrm{Al},1} &= O_1 \cdot \eta_{\mathrm{O}} \\
O_{\mathrm{Al},1} &= 0.31 \cdot 0.8 \\
\Delta m_{\mathrm{Al},1} &= \min\left\{\frac{O_{\mathrm{Al},1}}{0.623}, m_{\mathrm{Al},1}\right\} = \min\left\{0.3995, 5.5\right\} \\
&= 0.3995 \text{ kg}
\end{aligned}
$$

In case the remaining mass of aluminum is smaller than the theoretical amount to oxidize, the next element in the priority sequence (titanium) reacts with the left-over oxygen. The oxygen for titanium is then set to the left-over of the reaction with aluminum, without a second consideration of η_O due to the fact that the overall yield has already been considered. Based on the fact that the exemplary heat for the present illustrative example does not contain titanium, the next element in the sequence is silicon.

Since the total usage of oxygen by aluminum, the Algorithm 4.1 evaluates the conditional statement at line 7. The condition is described in the previous section with Equation (3.17). Thus, the calculation of $\delta_t^{\mathrm{start}}$, already with the consideration of the absence of titanium, evaluates to 1 according to:

$$
\delta_t^{\mathrm{start}} = \begin{cases} 1 \ldots (5.5 - 0.3995 + 55.0 - 0) \geq 0 \\ 0 \ldots \mathrm{otherwise} \end{cases}
$$

Afterwards, the model algorithm continues at line 18, the temperature balance calculation. The following descriptions evaluate the overall temperature balance referring to the lines 18 until 20. The implementation of the temperature balance evaluation is considered as described in Equation (3.9). The temperature gained by oxidation accounts for aluminum only, since the total amount of oxygen reacts with aluminum. The overall temperature calculation for $t = 1$ is carried out as follows:

$$\begin{aligned}\Delta T_{\mathrm{Al},1} &= \frac{\Delta m_{\mathrm{Al},1} \cdot \Delta H_{\mathrm{Al}}}{m_{\mathrm{metal},0} \cdot \mathrm{CP}} \\ &= \frac{0.3995 \cdot 31104000}{110000 \cdot 850} \\ &= 0.1329\,\mathrm{K}\end{aligned}$$

and for accounting the cooling due to the oxygen jet:

$$\begin{aligned}\Delta T_{\mathrm{jet},1} &= \frac{\mathrm{C}_1 \cdot O_1 \cdot (T_0 - 30)}{m_{\mathrm{metal},0} * \mathrm{CP}} \\ &= \frac{-1314.68 \cdot 0.31 \ldots \cdot (1590 - 30)}{110000 \cdot 850} \\ &= 0.0068\,\mathrm{K}\end{aligned}$$

followed by the evaluation of the pressure limit condition for the given time-step:

$$\delta_1^{\mathrm{p-limit}} = \begin{cases} 1 \ldots & P_1 \leq 800 \\ 0 \ldots & P_1 > 800 \end{cases}$$

$$\delta_1^{\mathrm{p-limit}} = 1$$

Finally, the temperature balance was formulated as:

$$\Delta T_1 = \frac{-T_{\mathrm{loss}} \cdot \Delta t}{60} - \frac{T_{\mathrm{loss-p}} \cdot \Delta t}{60} \cdot \delta_1^{\mathrm{p-limit}} + \Delta T_{\mathrm{Al},1} - \Delta T_{\mathrm{jet},1}$$

$$\begin{aligned}\Delta T_1 &= -0.0083 - 0.005 \cdot 1 + 0.1329 - 0.0068 \\ &= 0.1127\,\mathrm{K}\end{aligned}$$

After the calculation of the temperature balance, the entire algorithm terminated for $t = 1$ and $\Delta t = 1$. The last step is the update of the conditions according the single results of the calculations. An overview of the main results of the calculation step can be obtained by table 4.1.

Arbitrary Time-step

The illustration of the steps for $t = 1$ points out that the first steps until t_{start} is reached are only for oxidation of the priority elements. As with further calculations, t_{start} evaluates to be 191. In other words, after 191 seconds the model enters the main decarburization phase. This marks the beginning of carbon, chromium, manganese and iron oxidation. In order to demonstrate a more comprehensive calculation cycle, the following paragraph shows the calculations done for time-step $t = 1538$, where the critical carbon level has already been exceeded. That means, excessive oxygen amount based on the kinetic approach reacts additionally with chromium. Similar to the calculation cycle demonstrated for $t = 1$, the cycle start with the take-over of the variables:

$$O_{1538} = 1400\ \mathrm{m^3\,h^{-1}} = 0.388\ \mathrm{m^3\,s^{-1}}$$
$$P_{1538} = 130\ \mathrm{mbar}$$
$$S_{1538} = 50\ \mathrm{L\,min^{-1}} = 0.00088\ \mathrm{m^3\,s^{-1}}$$

Since the detailed calculations of the steel and slag activities were already illustrated above, for the current cycle the illustration continues with the evaluation of the kinetic decarburization rate $d\mathrm{C}, _{1538}$. Equation (3.4) states the calculation for the kinetic rate. But first, the β_{1538} is evaluated to be $\beta_1 = 0.004$ since $O_{1538} > 0$ is true, according to Equation (3.5). To calculate the necessary carbon in equilibrium condition, the results for $F_{\mathrm{CO},1538}$ and $p_{\mathrm{CO},1538}$ are calculated according to the Equations (3.7) and (3.14). The fact that $d\mathrm{C}_{1537}$ is greater zero as indicated above, the pressure correction is conducted as follows:

$$r_{\mathrm{CO},1538} = d\mathrm{C}_{1537} \cdot \frac{22.4}{12000} \cdot m_{\mathrm{metal},1537}$$
$$r_{\mathrm{CO},1538} = 0.2401 \cdot \frac{22.4}{12000} \cdot 109179.1$$
$$r_{\mathrm{CO},1538} = 489.82$$
$$p_{\mathrm{corr},1538} = \frac{489.822}{489.822 + 0.000833} = 0.9999$$

The obvious low influence of the stirring rate on the pressure correction will be investigated in the subsequent chapter. The additional pressure to be considered for the given

time-step results in:

$$p_{\mathrm{add},1538} = 10 \cdot -130^{20} = 0.01503$$

From this follows that p_{CO} at time-step 1538 is:

$$p_{\mathrm{CO},1538} = (130 + 0.01503) \cdot \frac{0.9999}{1000} = 0.13002$$

At second, the $F_{\mathrm{CO},1538}$ is computed using the results of the equilibrium calculations according to Equation (3.8):

$$\begin{aligned}
T_{1538} &= 1650.47 + 273.15 = 1923.62\,\mathrm{K} \\
\log K_{\mathrm{C}} &= \frac{1168}{1923.62} + 2.07 = 0.6071895 \\
K_{\mathrm{C},1538} &= 10^{0.6071895} = 475.5427 \\
\log K_{\mathrm{Cr}} &= \frac{44040}{1923.62} - 19.42 = 22.8943721 \\
K_{\mathrm{Cr},1538} &= 10^{22.8943721} = 2981.0695
\end{aligned}$$

Thus, $F_{\mathrm{CO},1538}$ is computed to:

$$F_{\mathrm{CO},1538} = \frac{12.7564^{\frac{2}{3}} \cdot 2981.0695}{0.55044 \cdot 475.5427 \cdot \sqrt[3]{0.345826}} = 0.4277$$

Based on the calculations above, the carbon in equilibrium at the given time-step can be obtained with:

$$eqm_{\mathrm{C},1538} = 0.4277 \cdot 0.13002 = 0.0556\,\%$$

At this point, the puzzle-pieces are completed and the kinetic decarburization rate for time-step 1538 can be finally calculated as follows:

$$d\mathrm{C}_{\mathrm{kin},1538} = 0.004 \cdot (0.1105 - 0.0556) \cdot \frac{109179.08}{100} = 0.2398\,\mathrm{kg}$$

According to Algorithm 4.1, the next step as indicated at line 10 is the conduction of the stoichiometric decarburization rate. This is necessary to evaluate the concrete decarburization approach for the present time-step. Therefore, the amount of oxygen is distributed

along the main elements carbon, chromium, manganese and iron as:

$$\begin{aligned}
O_{\mathrm{C},1538} &= O_{1538} \cdot \eta_O \cdot R_{\mathrm{C}} \\
&= 0.389 \cdot 0.8 \cdot 0.72 \approx 0.224 \\
O_{\mathrm{Cr},1538} &= 0.38\dot{8} \cdot 0.8 \cdot 0.17 \approx 0.0528 \\
O_{\mathrm{Mn},1538} &= 0.38\dot{8} \cdot 0.8 \cdot 0.1 \approx 0.031 \\
O_{\mathrm{Fe},1538} &= 0.38\dot{8} \cdot 0.8 \cdot 0.01 \approx 0.0031
\end{aligned}$$

Based on the oxygen distribution and the stoichiometric rate description of Equation (3.24), the computation is carried out as:

$$d\mathrm{C}_{\mathrm{sto},1538} = \frac{O_{\mathrm{C},1538}}{0.932} = 0.2403\ \mathrm{kg}$$

From this follows that the effective decarburization rate for the time-step 1538 is as follows:

$$d\mathrm{C}_{1538} = \min\{d\mathrm{C}_{\mathrm{kin},1538}, d\mathrm{C}_{\mathrm{sto},1538}\} = 0.2398\ \mathrm{kg}$$

The resulting oxidation for carbon in the present time-step is consequently based on the kinetic approach:

$$\Delta m_{\mathrm{C},1538} = 0.2398\ \mathrm{kg}$$

From this also results a left-over oxygen for the present time-step, which additionally accounts for the chromium oxidation. Based on the evaluation of the carbon oxidation for the present time-step, the other main elements are subsequently oxidized as follows:

$$\begin{aligned}
O_{\mathrm{left-over}} &= O_{\mathrm{C},1538} - (\Delta m_{\mathrm{C},1538} \cdot \nu_{\mathrm{C}}) \\
\Delta m_{\mathrm{Cr},1538} &= \frac{O_{\mathrm{Cr},1538} + O_{\mathrm{left-over}}}{\nu_{\mathrm{Cr}}} = \frac{0.0528\dot{8} + 0.0005184}{0.323} = 0.1653\ \mathrm{kg} \\
\Delta m_{\mathrm{Mn},1538} &= \frac{O_{\mathrm{Mn},1538}}{\nu_{\mathrm{Mn}}} = \frac{0.031\dot{1}}{0.204} = 0.1525\ \mathrm{kg} \\
\Delta m_{\mathrm{Fe},1538} &= \frac{O_{\mathrm{Fe},1538}}{\nu_{\mathrm{Fe}}} = \frac{0.0031\dot{1}}{0.201} = 0.0155\ \mathrm{kg}
\end{aligned}$$

At last, the temperature balance is evaluated equally with the previously described steps for $t = 1$. Although it is to mention that the temperature gain for the present cycle is made

up of all oxidized elements. This leads to a composed temperature balance of:

$$\Delta T_{1538} = 0.03147\,\mathrm{K}$$

Similar to the illustrative calculation example for the initial time-interval, the calculation cycle for time-step 1538 are summarized in Table 4.2. While Table 4.1 for $t = 1$ shows the chemical change in kg, Table 4.2 shows the evolution from $t = 1537$ to $t = 1538$ in weight-percent (wt-%) for better reading. Notably, the change in aluminum-oxide does not come from oxidation of aluminum during the calculation cycle, but due to the recalculation of the weight-percent balance. The kilogram of aluminum-oxide remain the same, as it can be computed by the total slag mass. However, any deviation is caused by rounded figures.

4.1.2 Feasibility Check of the Solution

As prerequisite to any result of the model, the exemplary solution (Figure 4.1) must meet the constraints. The following part illustrates the feasibility of the variables defined for the illustrative example.

In general, the process aims to reach a certain low carbon concentration at the end of the process. Referring to the first constraint described in the last section, the $\mathrm{C}_{\mathrm{target}}$ has been defined to be 0.005. By obtaining the final carbon content the constraint is fulfilled due to:

$$w_{\mathrm{C},3326} \leq \mathrm{C}_{\mathrm{target}}$$
$$0.00498 \leq 0.005$$

Regarding the oxygen flow, the constraints are defined as range of minimum and maximum oxygen flow for the complete pattern. Between t_0 and t_{start} the oxygen flow rate needs to be exactly 80% of the maximum flow. Dashed line series in Figure 4.1 mark the minimum-, maximum- and 80% of maximum flow rate along with the t_{start} point at $t = 191$.

Condition			t = 0	t = 1	Unit	Change
T_0	$\rightarrow$	T_1	1590	1590.1127	°C	$\uparrow$
$m_{tot,0}$	$\rightarrow$	$m_{tot,1}$	110000	109999.607	kg	$\downarrow$
$m_{\mathrm{Al},0}$	$\rightarrow$	$m_{\mathrm{Al},1}$	5.5	5.1	kg	$\downarrow$
$m_{\mathrm{Si},0}$	$\rightarrow$	$m_{\mathrm{Si},1}$	55	55	kg	-
$m_{\mathrm{C},0}$	$\rightarrow$	$m_{\mathrm{C},1}$	440	440	kg	-
$m_{\mathrm{Cr},0}$	$\rightarrow$	$m_{\mathrm{Cr},1}$	17930	17930	kg	-
$m_{\mathrm{Al_2O_3},0}$	$\rightarrow$	$m_{\mathrm{Al_2O_3},1}$	11.0	11.76	kg	$\uparrow$
$m_{\mathrm{SiO_2},0}$	$\rightarrow$	$m_{\mathrm{SiO_2},1}$	55.0	55.0	kg	-
$m_{\mathrm{Cr_2O_3},0}$	$\rightarrow$	$m_{\mathrm{Cr_2O_3},1}$	4.5	4.5	kg	-

Table 4.1: Results of the model calculation for the first time-step

Condition			t = 1537	t = 1538	Unit	Change
T_{1537}	$\rightarrow$	T_{1538}	1650.4668	1650.4983	°C	$\uparrow$
$m_{tot,1537}$	$\rightarrow$	$m_{tot,1538}$	109179.0783	109178.5134	kg	$\downarrow$
$m_{\mathrm{Al},1537}$	$\rightarrow$	$m_{\mathrm{Al},1538}$	0	0	wt-%	-
$m_{\mathrm{Si},1537}$	$\rightarrow$	$m_{\mathrm{Si},1538}$	0	0	wt-%	-
$m_{\mathrm{C},1537}$	$\rightarrow$	$m_{\mathrm{C},1538}$	0.1105	0.1103	wt-%	$\downarrow$
$m_{\mathrm{Cr},1537}$	$\rightarrow$	$m_{\mathrm{Cr},1538}$	16.2137	16.2136	wt-%	$\downarrow$
$m_{\mathrm{Mn},1537}$	$\rightarrow$	$m_{\mathrm{Mn},1538}$	0.9210	0.9208	wt-%	$\downarrow$
$m_{\mathrm{Al_2O_3},1537}$	$\rightarrow$	$m_{\mathrm{Al_2O_3},1538}$	2.5106	2.5092	wt-%	-
$m_{\mathrm{Cr_2O_3},1537}$	$\rightarrow$	$m_{\mathrm{Cr_2O_3},1538}$	39.6412	39.6482	wt-%	$\uparrow$
$m_{\mathrm{MnO},1537}$	$\rightarrow$	$m_{\mathrm{MnO},1538}$	31.2230	31.2293	wt-%	$\uparrow$
$m_{\mathrm{FeO},1537}$	$\rightarrow$	$m_{\mathrm{FeO},1538}$	3.7792	3.7795	wt-%	$\uparrow$
$m_{slag,1537}$	$\rightarrow$	$m_{slag,1538}$	852.0810	852.5395	kg	$\uparrow$

Table 4.2: Results of the model calculation for time-step 1538

The next constraints deal with the pressure capabilities of the equipment. According to the statements of the last section, the pressure at every time-step must be above $p_{\min} = 0.1$. The accomplishment of this constraint is also illustrated with dashed line series in Figure 4.1. In the same way, the pressure must be kept up to a certain level $p_{\text{main}} = 130$ during the main decarburization phase. The main decarburization phase has been calculated in the previous section from t_{start} until t_{crit}. Similar to t_{start}, the time-step of t_{crit} is marked in Figure 4.1. The calculation result of $t_{\text{crit}} = 1537$. At this point, the δ function expressed in Equation (3.24) evaluates to 0 for the first time and remain 0 until the end of the process. The conditions at $t = 1537$ are as follows:

$$d\mathrm{C}_{\text{kin},1537} = 0.2401$$
$$d\mathrm{C}_{\text{sto},1537} = 0.2403$$
$$w_{\mathrm{C},1537} = 0.1105$$

With this in mind it can be shown that $\delta_{1537}^{\text{main}}$ is zero since:

$$0.2101 > 0.2403 \wedge 0.1105 > 0.15$$

evaluates to false.

In order to ensure the requirements from domain experts, the oxygen flow rate, system pressure and stirring gas variables are not allowed to exceed 8 steps. This requirement is fulfilled by the results of:

$3 \leq 8$ for the oxygen flow rate

$3 \leq 8$ for the system pressure

$2 \leq 8$ for the stirring gas rate

This fact can also be visually obtained from the exemplary variables in Figure 4.1.

The last constraint defined in the previous section makes sure that the total amount of oxygen is at least enough to oxidize the priority elements and carbon until $\mathrm{C}_{\text{target}}$ based on plain physics. This constraint is defined by Equation (3.29) and can be proven as

follows:

$$
\begin{aligned}
&(5.5 \cdot 0.623 + 0 \cdot 0.468 + 55.0 \cdot 0.798) \\
&\quad + \left(440 - \frac{0.005}{100} \cdot 110000\right) \cdot 0.932 = 452.2705 \text{ m}^3 \\
&\qquad\qquad \sum_{t=1}^{5000} O_t \cdot 0.8 = 647.73 \\
&\qquad\qquad 647.73 \text{ m}^3 \geq 452.27 \text{ m}^3
\end{aligned}
$$

4.1.3 Evaluation of the Objective Function

In the previous subsection, two time-steps were calculated and explained in detail. Even more important, in order to rate the exemplary solution, which was chosen for the illustrative example, the objective function must be evaluated. Referring to the objective function of Equation (3.2), two requirements needs to be fulfilled:

1. Firstly, the calculation of each cycle from $t = 1$ until the end of the pattern is mandatory to assess the sum for the objective function. To accomplish the needs of the company for fast calculations of various solutions, the simulation tool which was already used for the parameter evaluation supports the calculation of predefined variable-patterns. Thus, the model simulation tool provides based given variable set a comma-separated values (CSV) file as output. The CSV file contains all calculated conditions and results for each calculation cycle, as it was described in the previous subsection.

2. Secondly, the parameter for t_{start} must be known. Due to the check on constraints in the first subsection of this chapter, the parameter was already conducted and is $t_{\text{start}} = 191$. In order to perform less calculations, the defined input parameter $t_{\max} = 5000$ is not necessarily required (i.e. when the final solution contains less variables). In case of the exemplary solution, the end turned out to be at $t_{\text{end}} = 3326$.

Based on the computation of all requirements for evaluating the objective function, it can be formulated as:

$$O_{\mathrm{Cr}} = \sum_{191}^{3326} (O_t \cdot \eta_O \cdot R_{\mathrm{Cr}} + k_t)$$

The required calculation for k_t was explained in the previous section, especially for the cycle $t = 1538$. Verbally, k_t can be expressed as the formation of chromium-oxide due to excessive oxygen (also called left-over oxygen). Excessive oxygen is in place, whenever the conditions favor the kinetic decarburization approach over the stoichiometric approach.

However, by contemplating the structure of the objective function, the evaluation of the resulting total mass of oxygen can be split into two parts. The first part covers the amount of oxygen, which the model always accounts for chromium. This part can be calculated as:

$$\sum_{191}^{3326} O_t \cdot \eta_O \cdot R_{\mathrm{Cr}} = 102.07 \text{ m}^3$$

The second part deals with the left-over oxygen whenever the kinetic approach is in favor. In other words, whenever $d\mathrm{C}_{\mathrm{kin},t}$ is lesser than $d\mathrm{C}_{\mathrm{sto},t}$. This relationship was demonstrated in the previous subsection and the deduction is shown in Equation (3.3). Consequently, the sum for the left-over oxygen is calculated as:

$$\sum_{191}^{3326} k_t = 69.73 \text{ m}^3$$

Finally, the initially questioned total amount of oxygen used for chromium-oxidation is:

$$O_{\mathrm{Cr}} = 102.07 + 69.73 = 171.80 \text{ m}^3$$

To summarize the plain numbers deduced from the result: 171.80 m^3 of oxygen means 531.90 kg of chromium is oxidized. The mass of chromium caused a final amount of 777.42 kg chromium-oxide formed in the slag area. The summary of the overall calculation process is shown in Figure 4.2. The figure shows the kinetic decarburization rate in red and the stoichiometric decarburization rate in blue. At the critical carbon t_{crit} the

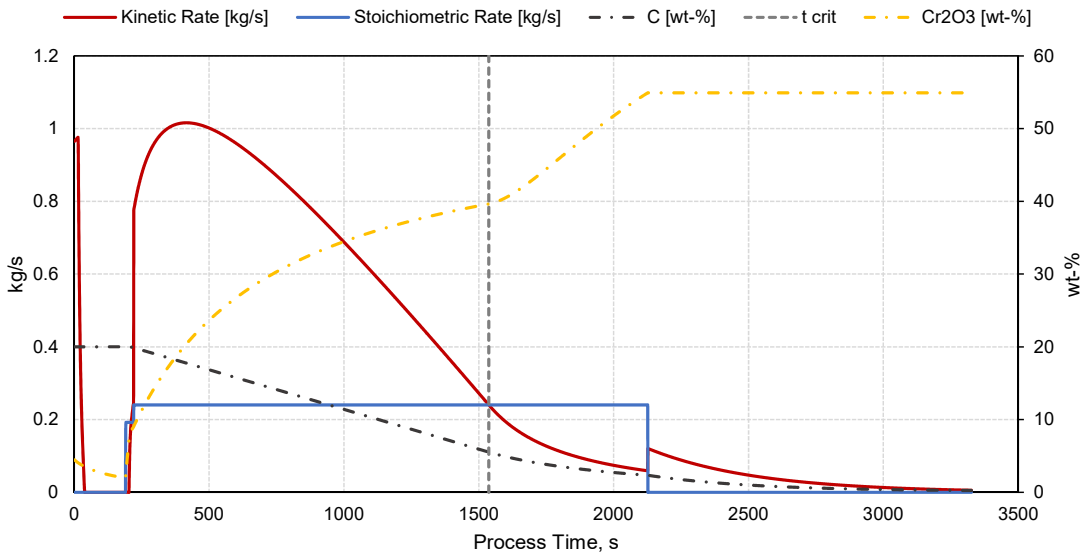

Figure 4.2: Results of the illustrative example focusing on carbon and chromium-oxide

yellow dashed line indicates the increase of chromium oxidation due to the excessive left-over oxygen. The black dashed line series shows the calculated carbon content.

4.2 Evaluation of Different Solutions Based on the Illustrative Example

Based on the results of the previous section, different solutions of variables will be executed and the different results are discussed and shown in the following. Before another solution can be discussed, the result of the illustrative example must be examined and understood in detail. The present section describes different modified solutions, in order to solve the same problem of the illustrative example, but with enhanced chromium oxidation.

4.2.1 Variables and Their Effect on the Solution

What was discussed throughout the present master's thesis can be visually obtained by Figure 4.2: the critical time-step is where the kinetic decarburization rate meets the stoichiometric rate and falls below henceforth. In addition, it is also obvious, that from this

moment on, the chromium oxidation increased significantly. The reason is the explained left-over oxygen, precisely because the kinetic rate is in favor. The strong increase of chromium-oxide at the beginning of the main phase is caused by the low start temperature. Referring to the Equations (2.19) and (2.20), the temperature relationship in the kinetic rate is explained. This temperature relationship causes the kinetic rate to be in favor and shifts the oxygen towards chromium in order to gain temperature at the beginning. Although the fact, that the shifting of 100% of oxygen towards carbon at the very specific time-step does not represent the reality, the influence of this implementation on the final result is correspondingly low. In fact, this implementation of the temperature relationship leads to more reliable results at all due to the indirect VOD start temperature consideration (see Section 2.3.4).

However, the significant increase of chromium-oxide after reaching the critical carbon t_{crit} seems to have potential for improvement. In advance of calculating the result of an improved solution, the possibilities of improvement must be determined. In fact, the optimization problem maintains three types of variables to "play" with (with respect to the constraints of the model):

- the oxygen blowing rate [$\mathrm{m^3\,h^{-1}}$],
- the system pressure [mbar] and
- the stirring gas rate [$\mathrm{L\,min^{-1}}$].

As pointed out in the illustrative example (calculation details of step 1538), the stirring gas rate had an obvious low influence in the calculation. In the AOD process the inert gas is used to decrease the partial pressure of CO. In the VOD process, this is realized by the system pressure, also named tank or vessel pressure. Since the present model does not account for the influence of stirring gas on the mass transfer coefficient and the area of reaction, the stirring gas rate had an obvious low influence in the illustrative calculation example.

For that reason, the present section focuses on the improvement of the oxygen blowing pattern by analyzing the oxygen blowing rate and the system pressure. The latter is mainly responsible for the kinetic rate, while the oxygen blowing rate is responsible for the oxidation at all.

4.2.2 Oxygen Blowing Rate Modifications

Without having an automatic optimization algorithm on the described model, by visually analyzing Figure 4.2, a manual improvement attempt is carried out. First of all, the check on constraints of the previous section pointed out, that much more oxygen is used than necessary based on plain physics. Combined with the observation of the excessive oxygen after t_{crit}, the first improvement attempt can be described as follows: the exemplary solution from the illustrative example has been modified to have a step for the final oxygen blowing phase after t_{crit}. Therefore, the last area is split into two equal parts. In other words, in the middle of the time after t_{crit}, the oxygen blowing rate is reduced to the minimum oxygen blowing level, which was defined to be 800 $\mathrm{m}^3\,\mathrm{h}^{-1}$.

Solution 2:
Figure 4.3 illustrates the calculated results of the first improvement attempt on the initial solution. Notably, the x-axis of the diagram is zoomed to the most interesting area, since the boil-off phase remained unchanged. At the first view, the results look promising compared to the initial solution. The step has decreased the formation of Cr_2O_3 as it can be visually obtained from the diagram. The calculated results in terms of numbers can be summarized as: $O_{\mathrm{Cr}} = 139.40$ m^3 oxygen dedicated to chromium with a final carbon concentration of $\mathrm{C}_{\mathrm{end}} = 0.00557\%$. The final temperature resulted to be 1662.60 °C. Although all required constraints were fulfilled in advance, the modification of variables lead to a higher carbon content as allowed after the calculation. This side effect must be considered when improving the variables manually. Due to the less oxidation of chromium, the temperature gain is proportionately lower. As a consequence, the kinetic rate is smaller since the moment of oxygen flow reduction. In other words, the smaller kinetic rate due to the lower temperature implies less carbon to be oxidized at this time.

Based on the findings, the improved solution needs to be re-worked again, to bring it back into the allowed range. In order to do so, the pattern must be extended to reach the final carbon content of 0.005. The setback of extending the blowing pattern is an increased time-period to oxidize chromium. Figure 4.4 shows the extended, but feasible according to all constraints, variable solution. At the end, the blowing pattern has been extended by 132 s, which is in fact 2.2 min. The final results of the first improvement on the initial

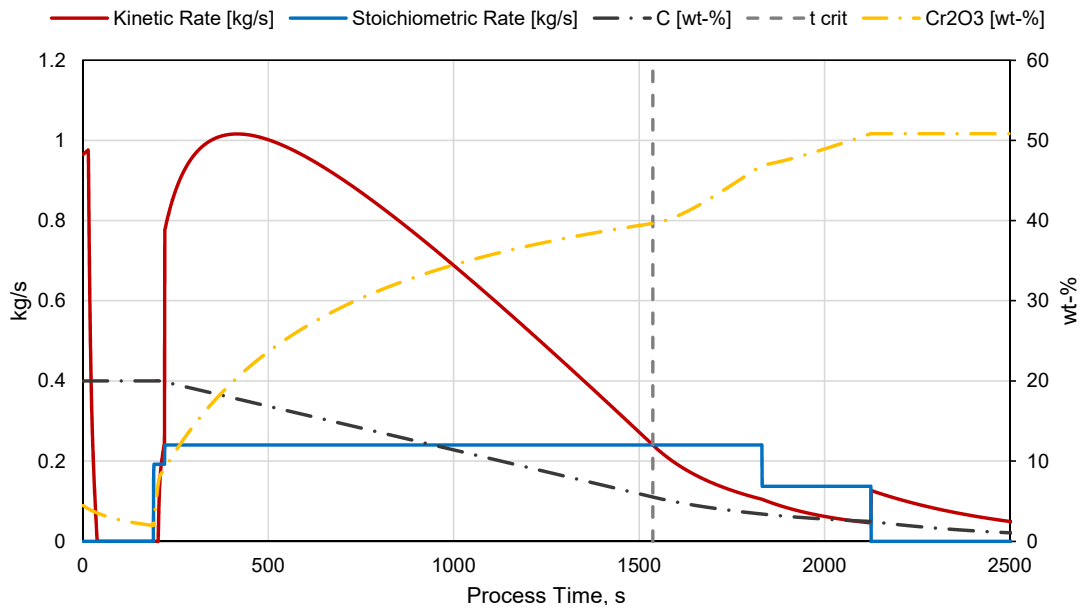

Figure 4.3: Evaluation results of the first improvement on the initial solution

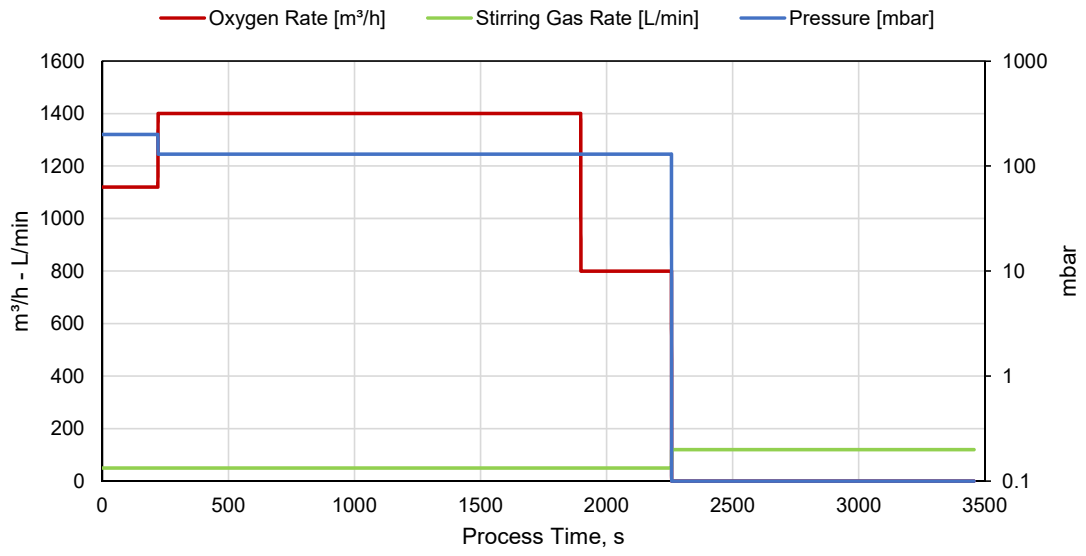

Figure 4.4: Corrected feasible variables of the first improvement on the initial solution

version are:

$$\sum_{191}^{3458}(O_t \cdot \eta_O \cdot R_{\mathrm{Cr}} + k_t) = 162.05 \text{ m}^3 \text{ O}_2$$

This result means about 10 m^3 less oxygen for chromium oxidation. Altogether, the result of the objective function means 501.70 kg of chromium oxidized to 733.28 kg of chromium-oxide. In comparison to the initial version, this means an improvement of $\tilde{4}4$ kg of Cr_2O_3.

Solution 3 and 4:
The logical next step is the further improvement of the second version. A close look to the diagram of Figure 4.3 still indicates excessive oxygen between the kinetic rate and the line of the stoichiometric rate. Thus, two further improvements are carried out in the following. The first contains two steps, whilst the second solution (fourth overall solution) contains four steps in total. Figure 4.5 compares solution three and solution four by focusing on the kinetic and stoichiometric rate. Clearly, the diagram points out that together with every additional final blowing step, the entire blowing pattern must be extended in order to reach the required carbon content. The dashed red line in Figure 4.5, which marks the four-step solution, is apparently lower than the solid red line of the three-step solution.

In order to summarize the modifications carried out so far briefly, the following list compares the results of the initial version shown in the illustrative example with all three improved solutions:

1. Illustrative example: 171.80 m^3 O_2
2. Modified solution 2: 162.05 m^3 O_2
3. Modified solution 3: 160.65 m^3 O_2
4. Modified solution 4: 159.52 m^3 O_2

Overall, all patterns could decrease the final chromium-oxidation. However, the tendency is obvious: the improvement between versions is getting less and less. To summarize, decreasing the area between the kinetic rate and the stoichiometric rate after the critical carbon level improves the solution without a doubt. At the same time, the difference

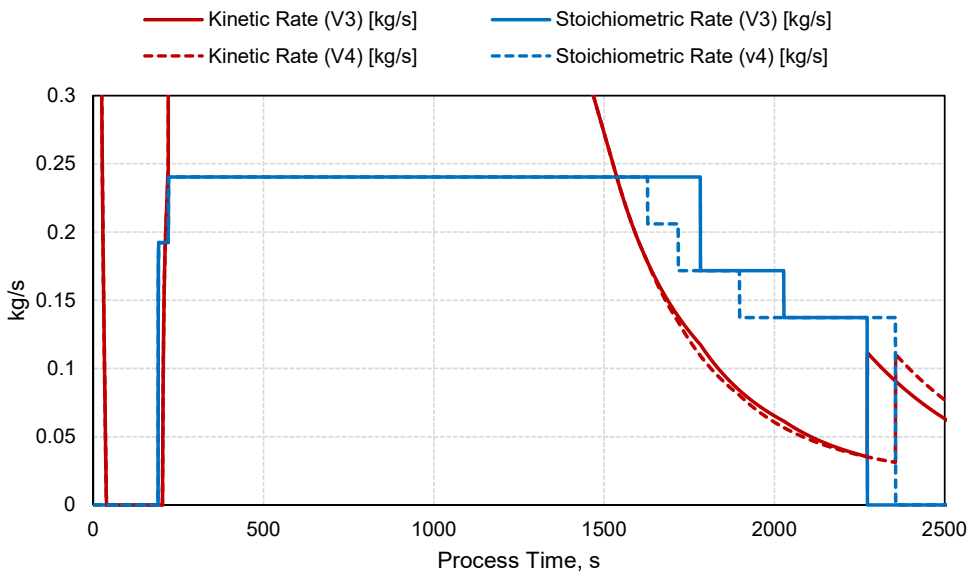

Figure 4.5: Oxygen rate improvement solution 3 and 4 in comparison

between introducing a single final step and four final steps is not significantly high, considering the drawback of extended treatment times. To make a step forward, the system pressure, which is together with the temperature mainly responsible for the kinetic rate, will be analyzed in the following subsection in order to examine further improvements.

4.2.3 System Pressure Modifications

Improvements based on adjusting the oxygen blowing rate is possible but as demonstrated not that successful at all. As described, the system pressure is mainly responsible for the kinetic rate, as well as the temperature. Furthermore, the figures above show all that the kinetic rate faces a drastic increase with the pressure reduction to 0.1 for the boil-off phase. Without any further knowledge, the relationship can be described as: the lower the pressure of the system, the higher the kinetic rate. According to metallurgists, the relationship is not as easy as that in reality. The detailed relationship between the system pressure and the kinetic rate incorporated in the model, is described in the metallurgical and model background section. Nonetheless, exactly this relationship must be used for further improvements.

As also described in the background section, the control of the system pressure is part of the equipment's capability. During the process, the equipment has to establish a certain

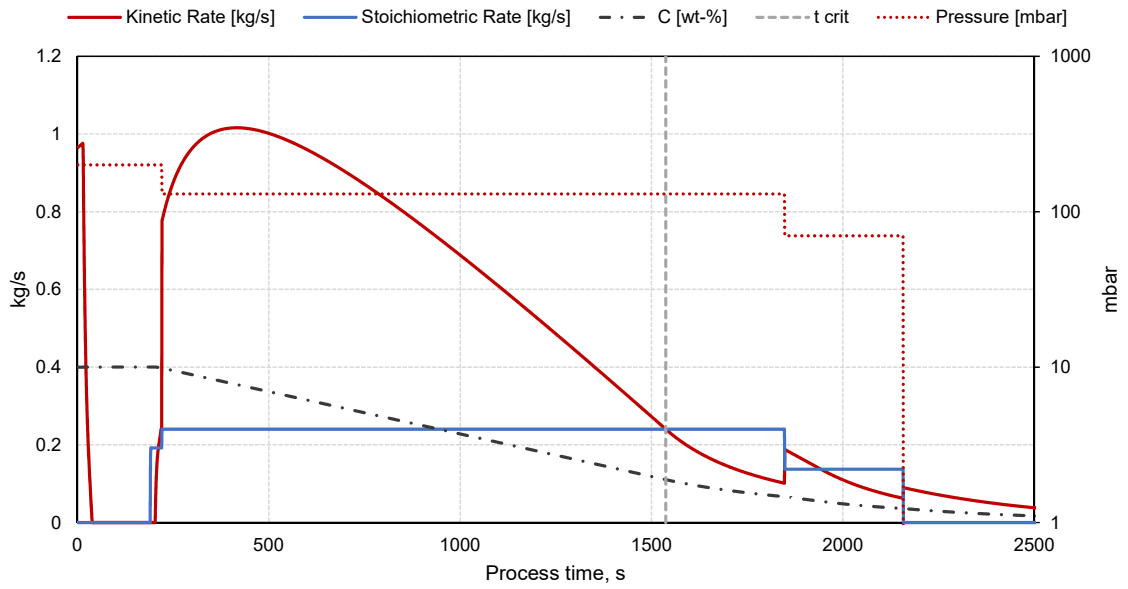

Figure 4.6: System pressure reduction on solution 5

pressure which is possible to achieve. This means, the oxidation of carbon during the main decarburization phase, considering an oxygen injection jet of 1400 $m^3\,h^{-1}$ does not allow a deeper pressure than defined as p_{main} = 130 mbar. Thus, the following solutions 5 and 6 assume a possible pressure reduction by reducing the oxygen injection rate.

Solution 5:

First of all, the effect of reducing the system pressure must be evaluated. Therefore, solution number two from the oxygen rate modifications is taken. Along with the oxygen flow reduction to 800 $m^3\,h^{-1}$, the system pressure is reduced to 70 mbar. Figure 4.6 shows the results of the calculation of solution number five. Similar to above, the diagram zooms the part of most interest and cuts off the boiling-phase. Additionally to the kinetic- and stoichiometric rate, the diagram shows the system pressure for a better illustration of the effect. As described, along with the oxygen blowing reduction, the pressure is reduced to 70 mbar. At the same time the kinetic rate faced an increase, so that for a short moment the stoichiometric approach was again in favor for decarburization. Finally, the pressure reduction makes it possible to reduce the time of the blowing pattern again. In fact, solution five is only 32 seconds longer than the illustrative variable pattern, but achieved the following improved results: 132.77 m^3 O_2; this means a reduction of approximately 39 m^3 O_2, which is at the end a reduction of approximately 176.6 kg Cr_2O_3.

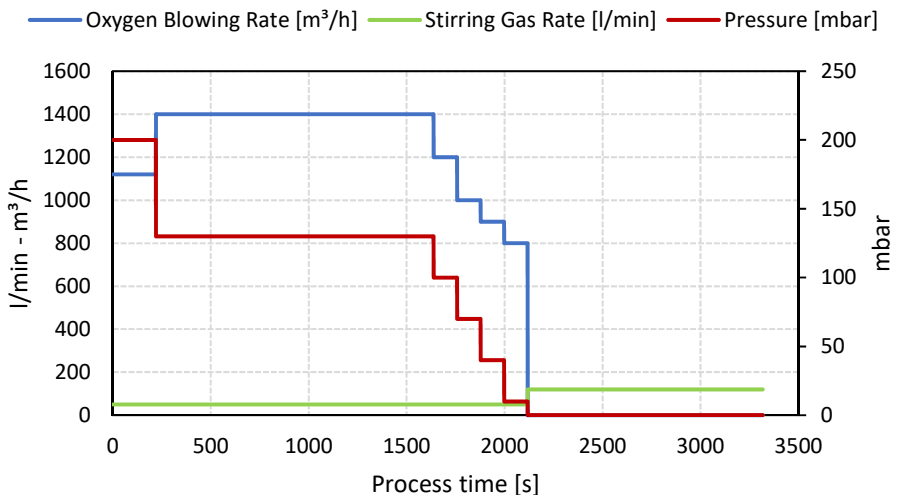

Figure 4.7: Combined solution of pressure and oxygen-rate reduction

Solution 6:

Based on the previous findings and the effect of the system pressure on the kinetic rate, a final solution can be carried out by combining the best results from the oxygen rate modifications and the findings of the system pressure effect. In other words, together with the four oxygen rate reductions, the pressure was reduced by 40 mbar respectively. Figure 4.7 shows the variables pattern for solution six. As illustrated in the diagram, the system pressure (red line series) is reduced along with the reduction of the oxygen flow rate (blue line series). The simultaneous reduction of oxygen and pressure is based on the assumption of reduced off-gas formation in the tank.

Finally, Figure 4.8 shows the conditions and results for solution six along the process time. The described effect of the system pressure on the kinetic rate calculation is visualized in Figure 4.8. With every step at the end, the stoichiometric rate decreases, while the kinetic rate increases. As a consequence, the area between the two series, stoichiometric and kinetic rate respectively, is smaller compared to any previous solution. Accordingly, this fact is also reflected by the calculated figures of the objective function:

- 108.86 m^3 O_2 (improvement of 92.94 m^3),
- which implies 337.03 kg Cr oxidized (improvement of 194.86 kg)
- and results in 492.60 kg Cr_2O_3 formed (improvement of 284.80 kg)

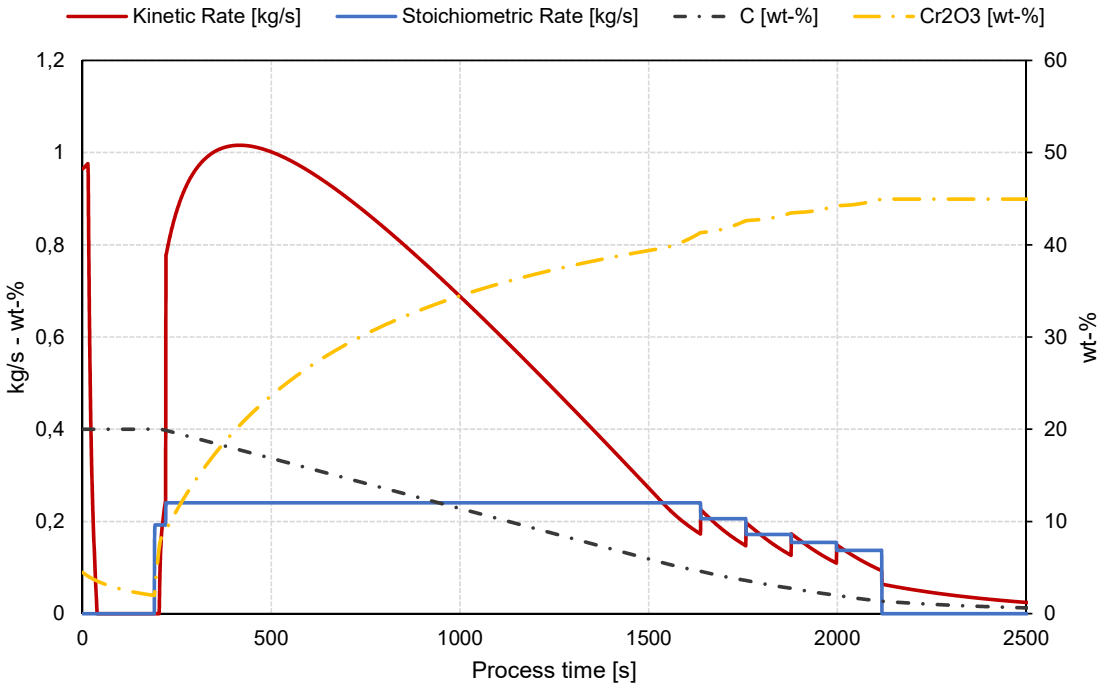

Figure 4.8: Calculation results of the combined solution of pressure and oxygen-rate reduction

4.3 Impact and Effects on the Optimization Problem

The described phenomena in the present chapter are focused on manual improvements. This methodology is used to identify the impacts on the final solution of the offline simulation model, which leads to a value of the objective function. By doing so, the oxygen blowing rate as well as system pressure modifications were carried out and compared. Thus, the fact finding study turned out that modifying the oxygen blowing rate after the critical carbon time-step does improve the solution. But, the achieved improvements are smaller the more final blowing steps are introduced. The drawback of more final blowing steps is the extended blowing time in order to reach the final necessary carbon content. Therefore, the successive fact finding study dealt with the modification of the system pressure. The tests on different solutions point out that the system pressure (together with temperature) has a significant effect on the kinetic decarburization rate, as described in the domain specific related work. Thus, a final solution was carried out by combining the advantages of oxygen rate and system pressure reduction. Based on the work up to now, the following chapter introduces an algorithm, to create an optimized variable pattern according to the input parameters.

5 Optimization Algorithm and Numerical Tests

The present chapter describes in detail a proposed algorithm according to the optimization model defined in Chapter 3 and the important findings of Chapter 4. Therefore, the present chapter is subdivided into two parts: (1) an overall description of the algorithm's concept and (2) a detailed description of the implemented source code.

5.1 Algorithm Concept

In order to find an appropriate algorithm for a various range of problems, the effects of the oxygen flow rate [$\mathrm{m}^3\,\mathrm{h}^{-1}$] and the system pressure [mbar] are of most interest. Therefore, based on the last combined solution of the previous chapter, the basic concept of the algorithm is to create a pattern, which follows this idea. In general, the algorithm must consider the same steps as the existing online model does. This means, according to the input parameters, the algorithm must follow similar steps than the online model. The necessary steps are summarized briefly:

- At first, the optimization algorithm must oxidize the priority elements Al, Si and Ti. This must happen at 80% of the maximum oxygen flow rate to meet the corresponding constraint of the optimization model.

- At second, the main decarburization phase must be carried out by using the maximum flow rate and at the pressure level defined with p_{main}.

- Thirdly, the final blowing phase must be defined. In particular, the final blowing phase can be defined as the oxygen blowing time after t_{crit} is reached. To remember, t_{crit} is reached, when the kinetic decarburization rate meets the stoichiometric

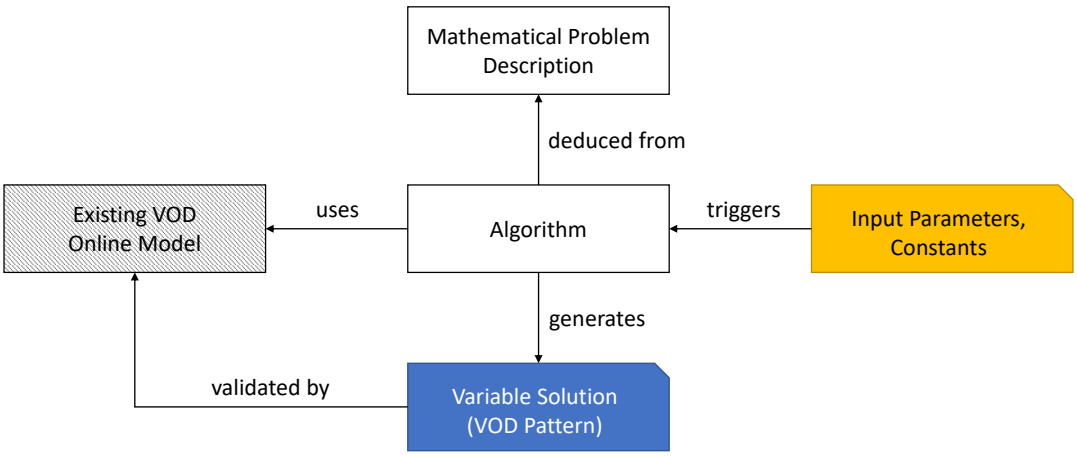

Figure 5.1: Schematic drawing of the optimization algorithm's basic concept

decarburization rate at a carbon level lower than 0.15%. The referring model description for the conduction of t_{crit} is defined in Equation (3.24).

When defining an optimization algorithm, the mathematical problem statement as described in Chapter 3 is the fundamental basis. With this in mind, the algorithm can verbally described as optimization tool to generate an oxygen blowing pattern, which meets all the constraints and minimizes chromium oxidation. Most importantly, the generated pattern meets the constraints as described. The oxidation of carbon until a defined input parameter is the key constraint. Moreover, the input parameters of the algorithm can be obtained from the dedicated section within the mathematical problem statement (see Chapter 3).

The concept of the optimization algorithm is strongly based on reusing the library of the already verified online model. The mathematical problem statement was already carried out by examining the online model. Thus, the reuse of the given library is standing to reason. Figure 5.1 illustrates schematically, what is described so far: based on the mathematical problem statement, the concrete implementation of an optimization algorithm is carried out. Nonetheless, the mathematical description of any optimization problem is essential. In addition, the implemented algorithm uses the existing library to generate the VOD pattern (solution of variables). Based on the basic concept described, the following sections describe in detail the implemented optimization algorithm followed by numerical tests.

5.2 Description of the Implemented Optimization Algorithm

The optimization algorithm is developed using the programming language C#. In fact, the following description of the implementation is independent of any programming language. However, due to the concept of reusing existing packages of the online model, choosing the same programming language for easy incorporation is reasonable. Besides, the programming style/language or software architectural considerations are not part of the thesis. The developed algorithm focuses on solving the optimization problem. The structure of the present section sees the algorithm at first and the detailed description of the main parts at second. Thus, Algorithm 5.1 illustrates the implemented optimization code from a high-level pseudo-code perspective.

As pointed out in the previous section, the implemented code is structured to perform the necessary steps sequentially. Firstly, the oxidation of the priority elements is carried out. Secondly, the main decarburization phase is defined until the critical carbon point is reached. Up to this certain point, all the steps are simply calculated and deduced from the mathematical problem statement. From this point on, the method changed: an iterative solution finding principle is necessary. This means, the steps from line 7 until line 14 are repeated until the resulting pattern reaches the required constraints, especially the carbon target constraint. The iteration mainly determines the time for the final blowing steps. By increasing the time, the resulting pattern is extended. The loop breaks, whenever the carbon content reaches the target. Afterwards, the algorithm performs the concrete final blowing phases based on the determined time. Likewise, the required final blowing steps are performed. Finally, the generated results are summed up to the final solution pattern. The following subsections describe these steps more detailed.

5.2.1 Oxidation of the Priority Elements

After reading and parsing the input data, the oxidation of all possible priority elements comes first. This means, based on the content of Al, Ti and Si within the input data, the algorithm sets the variables accordingly, until all these elements are oxidized. This means in this case 80% of the maximum oxygen flow rate $O_{\max}$ [$m^3\,h^{-1}$], which is served as an input parameter. The present thesis up to now, used the same maximum flow rate

Algorithm 5.1 Overview of the algorithm to optimize the VOD process

1: read input parameters from configuration file
2: read model constants
3: oxidize priority elements
4: **while** $t < t_{crit}$ **do**
5: main decarburization phase
6: **end while**
7: **while** target carbon content not reached **do**
8: try 4 final blowing steps for D seconds, with $i = 1, \ldots, steps$
9: try boil-off phase
10: **if** carbon content higher than target **then**
11: increase D to extend blowing pattern
12: **end if**
13: **end while**
14: final blowing phases for determined D seconds, with $i = 1, \ldots, steps$
15: write generated pattern

throughout the explanations for replicability. However, the developed algorithm implementation is open for various settings for different VOD equipment.

Algorithm 5.2 shows the initial blowing step in detail. The algorithm sets the variables for this step as long as the mentioned elements, expressed by their masses, are completely oxidized. Equation (3.17) is the underlying relationship to the objective function. The calculations itself are executed by the existing library. Thus, the created variables will be handed over to the library as stated in line 3 of the algorithm. The difference compared to the previous variable study is, that instead of reading records from a file, the records are created based on the conditions. Besides the initial heat condition, the only input parameter necessary at that time is the maximum flow rate of oxygen $O_{\max}$. Notably, the system pressure and stirring gas rate are set to fixed values based on the average figures of the process in real-life. However, for further flexibility these values can be introduced as input parameters as well.

Algorithm 5.2 Detailed steps of the priority elements oxidation algorithm

1: **while** $m_{\mathrm{Al},t} + m_{\mathrm{Ti},t} + m_{\mathrm{Si},t} > 0$ **do**
2: set variables to $O_t = 0.8 \cdot O_{\max}$, $P_t = 200$ and $S_t = 50$
3: call model library
4: update results for mass and chemistry
5: **end while**

5.2.2 Main Decarburization Phase

The main decarburization phase is similar to the previous one. As described in the mathematical background section, the main decarburization phase lasts until time-step t_{crit}. Thus, the conduction of t_{crit} is crucial for the optimization algorithm. The information to determine this time-step can be obtained by Equation (3.24). Consequently, the optimization algorithm performs the main phase until the kinetic rate meets the stoichiometric rate. At the same time, the calculated carbon content must be below the introduced figure of 0.15%.

Algorithm 5.3 illustrates the implemented algorithm in a detailed way. Similarly to the oxidation of the priority elements, the algorithm hands over the created records until the described condition is reached. Next to $O_{\max}$, the second parameter used was p_{main} to specify the system pressure during this phase.

Algorithm 5.3 Detailed steps of the main decarburization phase

1: **while** $dC_t^{kin} > dC_t^{sto} \vee w_{\mathrm{C},t} > 0.15$ **do**
2: set variables to $O_t = O_{\max}$, $P_t = p_{\mathrm{main}}$ and $S_t = 50$
3: call model library
4: update results for mass and chemistry
5: extract current kinetic and stoichiometric rates
6: **end while**

5.2.3 Boil-Off Phase

Unlike the sequence of the pattern, the boil-off phase is implemented and explained. The reason is simply the usage of the boil-off algorithm during the final blowing phase calculation. Thus, the explanation of the boil-off phase is in advance. In terms of algorithmic code, the boil-off phase is implemented straight forward based on one input parameters: the maximum process time. Thus, the algorithm must call the library until whether the maximum process time $t_{\max}$ or the carbon target $\mathrm{C}_{\mathrm{target}}$ is reached.

The aim of the boil-off phase is the final decarburization by the use of the lowest pressure possible. Therefore, the variables for the boil-off phase are zero oxygen injection, minimum system pressure as defined with parameter $p_{\min}$ and likewise a static stirring gas rate at 120 $\mathrm{l\,min^{-1}}$. Finally, at this point the algorithm can either terminate with the target carbon content, or not. Both within the given maximum time range. If the target

carbon content is not reached, the referring first constraint of Equation (3.20) is not fulfilled. Consequently, an error to the caller is presented. Algorithm 5.4 shows the detailed steps of the boil-off phase.

Algorithm 5.4 Detailed steps of the boil-off algorithm

1: **while** $t < t_{\max} \wedge w_{\mathrm{C},t} > \mathrm{C}_{\mathrm{target}}$ **do**
2: set variables to $O_t = 0$, $P_t = p_{\min}$ and $S_t = 120$
3: call model library
4: update results for mass and chemistry
5: **end while**

5.3 Iterative Approach for the Final Blowing Phase

To meet the required constraints, the algorithm must define the last blowing steps appropriate, so that at the end of the boil-off phase the target carbon content is reached. In order to do so, the algorithm uses an iterative solution approach. This means, the final pattern will be defined and extended until the oxidation trial including boil-off phase reaches the target carbon content.

Before the final blowing phase and afterwards (boil-off phase), everything is calculated based on the mathematical equations defined. Based on the variable study, it is also obvious that the final blowing phase is crucial to minimize the chromium oxidation. However, since the kinetic decarburization calculation does not only depend on the system pressure but also on the temperature and on the previous decarburization rate, it is obviously difficult to calculate a final blowing pattern at a stroke. Therefore, an empirical iterative approach is selected to solve the problem, strongly based on the findings of the variable study (see Chapter 4).

The first consideration based on the findings is the reduction of pressure and oxygen flow at a time. Hence, the algorithm is based on the step-wise reduction of the pressure and oxygen flow, as illustrated in the last solution of the variable study (see Figure 4.7). Considering the defined limitation of pressure and oxygen flow reductions, the maximum allowed steps within a pattern is 8, as defined in Equations (3.26) to (3.28). Thus, the implemented algorithm can generate at maximum 5 steps at the end, to always ensure the constraints. In more detail, the implemented approach can be briefly described as follows:

Firstly, to instruct the algorithm the creation of a certain number of steps, a new input parameter N is introduced.

$$N = 1, \ldots, 5$$

Secondly, the initial final blowing duration D for each step is set to 30 seconds. Before setting the variables for a specific time-step, the algorithm calculates the Δ oxygen blowing according to the number of steps:

$$\Delta O = \frac{O_{\max} - O_{\min}}{N}$$

From this follows that the oxygen rate for each specific step of the final blowing phases

$$i = 1, \ldots, N$$

is implemented as:

$$O_t = O_{\max} - \Delta O \cdot i \quad \text{with} \quad t = t_{\text{crit}} + (i-1) \cdot D, \ldots, t_{\text{crit}} + i \cdot D$$

In case of the system pressure, a similar approach is used to determine the reduction for each step i:

$$\Delta P = \frac{p_{\text{main}} - 10}{N}$$
$$P_t = p_{\text{main}} - \Delta P \cdot i \quad \text{with} \quad t = t_{\text{crit}} + (i-1) \cdot D, \ldots, t_{\text{crit}} + i \cdot D$$

The stirring gas rate S_t is set to a fixed value of 120 $\mathrm{l\,min^{-1}}$ due to recommendations of metallurgists. As pointed out in the variable study, the stirring gas rate has no considerable influence on the result due to the make-up of the model.

These definitions lead to the variables for each step at the time-step t. The important part of the algorithm is to execute the model library on a trial basis. In other words, the final steps as well as the boil-off phase are executed for the reason to check if the variables hit the carbon target content or not. If yes, the algorithm generates the pattern with the variables that passed the test, otherwise the final blowing time gets increased by

10 seconds. At this point the trial starts over. This steps are repeated until the variables produce a feasible result or the algorithm exits after 50 iterations without a solution.

Algorithm 5.5 illustrates the implemented steps. Line 3 indicates the main loop of the iteration approach. For the iterations, a test object must be created since the results of the model library cannot be used directly. It is important to mention that the test object must be created with the same conditions which are calculated until t_{crit}. To put it differently, it must be assured that every trial iteration starts with the same conditions that occur after the main decarburization phase. Afterwards, the final blowing phase with the predefined time is going to be tested. Therefore, inside the first loop the variables with the reduced oxygen flow and system pressure is created (as described above). The next loop executes the variables by calling the model library until the predefined time. The next step is the execution of the boil-off phase with the test object. At last, the algorithm obtains the results of the test object and verifies the constraint as described. The check performed at line 16 indicates whether another iteration is necessary or the calculation has finished. Finally the algorithm terminates as soon as either the carbon check is true or the loop counter is 50. As indicated in line 21, the algorithm generates the variables according to the last final blowing time.

Algorithm 5.5 Detailed steps of the iterative final blowing phase

```
 1: set final blowing time D = 30 seconds
 2: set loop counter to 1
 3: while w_{C,t} > C_target and loop counter < 50 do
 4:    initialize test object for iteration
 5:    set step counter i = 1
 6:    while i ≤ N do
 7:       set variables for step according to i
 8:       while time counter <= D do
 9:          call model library
10:          update test object for mass and chemistry
11:       end while
12:       increase step counter i = i + 1
13:    end while
14:    call boil-off algorithm with test object
15:    obtain w_{C,t} of test object
16:    if w_{C,t} > C_target then
17:       increase final blowing time D = D + 10
18:       increase loop counter by 1
19:    end if
20: end while
21: create final-blowing steps according to last used final blowing time
```

5.4 Numerical Tests and Results

For the purpose of evaluation of the developed algorithm, the present section performs various numerical tests. Therefore, the developed and described algorithm is used with the identical parameters as introduced in the mathematical problem statement and also used in the variable study (see Chapters 3 and 4). The numerical tests of the present section are carried out as follows:

- Firstly, the initial input parameters of the variable study (illustrative example) are used to create a solution based on the algorithm.
- Secondly, these input parameters are taken, but slightly modified regarding the start carbon concentration to demonstrate the function of the algorithm.
- Thirdly, the initial input parameters are taken again, but the start carbon concentration is modified to a specifically higher, and lower start value. This step is performed to indicate that the algorithm also generates a solution for carbon contents at the outer ranges of typical inbound VOD steels.
- Finally, four selected test heats, taken from from the customer in the field, are tested and compared. The chemistry of these steels along with the verified parameters serve as input for the algorithm.

For the sake of comparison of the impact of different final steps N on the model result, all tests are calculated for N is 3, 4 and 5 final blowing steps. The following sub-sections describe the simulations and tests regarding predefined input data as well as a comparison of generated control strategies for real process data carried out in the field.

5.4.1 Tests and Results Using Predefined Input Data

As mentioned in the introduction of the present section, various numerical simulations are carried out. The first samples are taken and derived from the initial parameters, which are already used in the illustrative example. This ensures a comprehensive comparison with the same input parameters. Additionally, to demonstrate the capability of the algorithm, derived input parameters are defined, modified only in terms of the start carbon concentration:

1. Illustrative example
   Although already introduced in the mathematical problem statement, the input parameters are 110000 kg at 1590 °C and the chemical composition for the illustrative example is as follows:
   C = 0.400%, Si = 0.05%, Mn = 1.2%, P = 0.025%, S = 0.005%, Cr = 16.3%, Mo = 2.0%, Ni = 10.1%, Cu = 0.28%, Al = 0.005%;
   Likewise, the initial slag mass is 100 kg and its composition is defined to be:
   CaO = 45%, SiO_2 = 23%, MgO = 9%, Al_2O_3 = 11%, FeO = 5.5%, MnO = 2%, Cr_2O_3 = 4.5%;

2. Similar start carbon
   The main parameters such as steel weight, slag weight and temperature remain the same as described above. The only modification is for the carbon concentration. The concentration is changed to a similar value as the initial version: C = 0.500%.

3. High start carbon
   The high carbon test data includes the same parameters as introduced above, but moves the carbon content to the higher level. The inbound carbon content of the VOD process mostly depends on the ladle furnace treatment before. In other words, it is possible to start the VOD process facing an extraordinary high carbon content. For the numerical test, the carbon content is changed to C = 0.700%.

4. Low start carbon
   Similarly as the high carbon test, the low carbon example covers inbound steels with lower inbound carbon levels. Whenever a VOD treatment for extremely low carbon steels is required, alloying operations in advance often do not consider carbon. Low range carbon around 0.2% is therefore possible. Thus, the carbon content is set to C = 0.200% for this test sample.

The different data-sets described above serve as input for the optimization algorithm. Firstly, the algorithm generates a control strategy for a 3-, 4- and 5-step final blowing phase. Secondly, the existing model evaluates the solutions by its replay function. This replay or simulation of the generated pattern leads to the result of the objective function per pattern. The results together with the chromium losses are shown in Tables 5.1, 5.2 and 5.3. Importantly, each table represents the results according to number of generated final steps. In other words, Table 5.1 shows the results for the 3-step generated patterns,

Input Data	T, °C	C	Cr	End Cr (O)	End Cr (3)
Illustrative Example	1590	0.400	16.30	16.013	16.168
Similar Start Carbon	1590	0.500	16.30	-	16.169
High Start Carbon	1590	0.700	16.30	-	16.110
Low Start Carbon	1590	0.200	16.30	-	16.122

Table 5.1: Algorithm simulation results for predefined input data (3-steps)

Input Data	T, °C	C	Cr	End Cr (O)	End Cr (4)
Illustrative Example	1590	0.400	16.30	16.013	16.170
Similar Start Carbon	1590	0.500	16.30	-	16.168
High Start Carbon	1590	0.700	16.30	-	16.108
Low Start Carbon	1590	0.200	16.30	-	16.121

Table 5.2: Algorithm simulation results for predefined input data (4-steps)

Table 5.2 the 4-step pattern results and Table 5.3 contains the results of 5 final blowing steps. Notably, the final chromium content is available for the illustrative example only (number 1), due to the fact that the other input parameters have been defined above for demonstration purpose, without the existence of an original zero-step pattern. Nonetheless, the column "End Cr (O)" refers to the end chromium content of the original blowing pattern. On the contrary, the column "End Cr (N)" refers to the end chromium content of the generated pattern, with N as the number of final steps respectively.

By comparing the results of the 3-, 4- and 5-step solutions for the illustrative example and the derived input data, the results do not show a significant difference. For example, the result of the illustrative example shows its best result with 4 final steps. The input data with similar start carbon with 3 final steps. Although the start carbon content of these two samples is similar, the best solution varies. The high start carbon sample shows its best performance with 5 steps. The reason for this observation can be explained by the way the algorithm is implemented. In other words, how it defines the final blowing steps. Since the algorithm uses the required number of steps as divider for the calculation fo the oxygen blowing rate and pressure reduction, the amount of reduction depends on the

Input Data	T, °C	C	Cr	End Cr (O)	End Cr (5)
Illustrative Example	1590	0.400	16.30	16.013	16.165
Similar Start Carbon	1590	0.500	16.30	-	16.163
High Start Carbon	1590	0.700	16.30	-	16.111
Low Start Carbon	1590	0.200	16.30	-	16.120

Table 5.3: Algorithm simulation results for predefined input data (5-steps)

number of steps. To put it differently, when reducing the system pressure with 3 steps, each step reduces the pressure by 40 mbar, whereas a 5-step solution reduces each step by 24 mbar. These figures can be obtained by the definition of the Algorithm 5.5. Consequently, in a 3-step solution, the increase of the kinetic rate per step is higher than in a 5-step solution. Finally, based on this allover distributed reductions, the different solutions lead to similar results. In this case, the algorithm or the model itself must consider more phenomena to come to a final conclusion. However, for the present thesis and focusing on the results itself, the calculated figures of the 4-step solution are selected for interpretation:

- Illustrative example: 104.37 m^3 O_2 indicates, that the optimization algorithm improves the best manual optimization by another 4.49 m^3. In order to compare the data-sets with different start carbon levels, the chromium loss can used for explanation. With the initial parameters, the algorithm achieves a final concentration of 16.17% chromium, which means a loss of 0.13%.

- Similar start carbon: the 0.5% carbon data-set shows a reasonably higher result of 137.94 m^3 O_2. The final chromium content is calculated to a final concentration of 16.17%. In this case a chromium loss of 0.13% is conducted.

- High start carbon: like the previous results, the 0.7% carbon data-set shows an increased oxygen amount of 179.40 m^3. At the same time, the result of the objective function means a final chromium content of 16.11%. Considering the extended pattern, this result means an improved chromium oxidation. The explanation is based on the higher carbon content: the kinetic rate depends on the temperature, which is higher due to the higher amount of carbon oxidation.

- Low start carbon: unlike the previous tests, the low carbon steel shows the worst result. The objective function results in 109.66 m^3 O_2, which is 5.29 m^3 more than the illustrative example. But also this result can be explained by the carbon content. Due to the low start temperature, the oxidation is generally in favor of chromium. With such low carbon levels, paired with a low start temperature, the generation of such a pattern might be questioned. Based on the experiences of metallurgists, a chemical heating treatment is often used. This can be understood as the addition of aluminum in advance. Consequently, at the beginning a significantly higher temperature is gained due to the aluminum oxidation. In case of a ladle furnace

in advance, the steel typically arrives already in a better temperature window for a VOD treatment.

5.4.2 Results and Comparison of Real Process Data

The data-sets derived from the illustrative example of the previous section provide a numerical but abstract impression of the enhanced patterns. Therefore, the present section selects four heats carried out in the field to simulate and compare the process data with the theoretical generated control strategy of the algorithm. The process data shown in Table 3.1 from Chapter 3 contain all the information to generate a control strategy by using the optimization algorithm. Based on the complete data-set illustrated in Table 3.1 the mentioned four samples are selected. Since the process data from the field covers the complete treatment at the equipment and not only the VOD related time-frame, the preparation of the simulation data to compare it with a generated control strategy is comparably time-intensive. However, for illustrating the effect of the algorithm on real process data from the field, four samples are simulated and discussed. The selection of the four samples is based on the smallest deviation between the measured and calculated carbon content by the model. In other words, those samples are taken where the online model showed the best performance during the real operation. Referring to Table 3.1, the heats with numbers 1 to 4 are selected.

At first, by using the implemented algorithm, an optimized solution is generated for each of the four steel grades. In a further step, the generated patterns are used as input for the offline function of the model. Thus, the chromium-oxidation which means the result of the objective function can be obtained for each generated solution. The resulting figures of the calculations are listed in the Tables 5.4, 5.5 and 5.6. For the sake of completeness also the simulations for the real heats comprise a 3-, 4- and 5-step solution. Similarly, the three tables show the results for the numbers of final blowing steps respectively. Besides, the tables do not only show the result of the chromium content comparison but also the start contents. The temperature, carbon and chromium in the first columns are the input parameters for the model. The parameters are shown in order to illustrate the range of the four steel grades selected. In a further column, the achieved chromium content, by simulating the original process data in the field is displayed. The column "End Cr (O)" is indicates the original end chromium content. Similar to the previous section, the last

#	Steel	T, °C	C	Cr	End Cr (O)	End Cr (3)
1	S316L	1625	0.360	15.77	15.43	15.580
2	F51	1585	0.647	22.23	21.98	22.031
3	S316L	1632	0.290	16.43	16.18	16.224
4	S316L	1557	0.330	16.13	15.70	15.754

Table 5.4: Algorithm simulation results for real process data (3-steps)

#	Steel	T, °C	C	Cr	End Cr (O)	End Cr (4)
1	S316L	1625	0.360	15.77	15.43	15.585
2	F51	1585	0.647	22.23	21.98	22.038
3	S316L	1632	0.290	16.43	16.18	16.221
4	S316L	1557	0.330	16.13	15.70	15.759

Table 5.5: Algorithm simulation results for real process data (4-steps)

chromium column "End Cr (N)" represents the final chromium content of the generated pattern, thereby the number in parenthesis marks the final steps of the solution.

As already observed in the previous simulations and tests, the different numbers of final blowing steps do not show a reasonable deviation. Three of the four simulated steel grades show the best results with the 4-step blowing pattern. As already described in the previous section, the algorithm overall divides the reduction over the final blowing phases. Thus, the resulting area between the stoichiometric rate and the kinetic rate remains similar, which leads to similar results of the calculation. Henceforth, the results of the 4-step simulation will be discussed in detail. According to Table 5.5, every steel grade of the four simulated samples show an improvement. The decreased chromium oxidation compared to the original control strategy can be obtained by the higher end chromium content. As an average, the generated control strategy for the heats of Table 5.5 improves the original on a modeling basis by 0.05 wt-% in the end chromium content. Taking the average of 110000 kg and the average range of chromium of 16% this number means a saving of approximately 55 kg of chromium. Especially for heat number two even more due to the higher percentage of chromium concentration. 55 kg Cr is equal to approximately 80

#	Steel	T, °C	C	Cr	End Cr (O)	End Cr (5)
1	S316L	1625	0.360	15.77	15.43	15.573
2	F51	1585	0.647	22.23	21.98	22.037
3	S316L	1632	0.290	16.43	16.18	16.227
4	S316L	1557	0.330	16.13	15.70	15.754

Table 5.6: Algorithm simulation results for real process data (5-steps)

kg of Cr_2O_3. The amount does not seem to be as high as for the predefined simulation tests. On the one hand, the first algorithm based on an optimization problem according the chromium minimization leaves room for improvements. On the other hand, as a next field of research, the generated control strategies must be practically evaluated and examined on real heats. However, also tests on real heats are difficult to carry out since the preparation of the exact same conditions for different blowing patterns is hard to set-up.

For the purpose of a better illustration of the enhanced results from the algorithm, a graphical comparison is created. Therefore, the sample data of heat number 1 is taken and compared to the generated pattern. The diagram of Figure 5.2 shows the simulation of the original process in the field. The full stroke series show the blowing pattern, while the dashed series illustrate the calculated conditions of the kinetic and stoichiometric decarburization rates. Notably, the stirring gas rate is spared-out in the diagram for better readability, and because the stirring gas rate does not influence the results of the model as described at the variable-study. The second diagram shown in Figure 5.3 illustrates the replay simulation of the optimized pattern. Again, the full stroke series are the variables of the generated pattern and the dashed series are the calculated conditions of the decarburization rates. The effect of less chromium oxidation, which is pointed out in Table 5.5, can be visually obtained by the comparison of the diagrams. The area between the kinetic and stoichiometric rates is significantly higher in the diagram of the original process. This leads to the result of lesser amount of oxygen used for chromium-oxidation in the optimized pattern. As discussed by the results of Table 5.5, the improvement based on the optimization algorithm can be visually obtained. Especially at the beginning, the control strategies follow an obviously different approach. Since the optimization algorithm has only the constraint of 80% of the maximum blowing rate $O_{\max}$ for the oxidation of Al, Si and Ti, the real operation follows a slower step-wise approach at the beginning. This approach is based on further considerations of metallurgists, which is not incorporated in the constraints of the optimization problem. Thus, in the first part of the main decarburization, the model oxidizes more carbon in the optimized pattern. As a consequence, the optimized control strategy is shorter in treatment time. Although both diagrams scaled the x-axis to 70 minutes process time, the optimized pattern reaches the required carbon content at 62 minutes, whereas the original blowing pattern stops the boil-off phase at 67.5 minutes. Clearly, by comparing the two diagrams the results of the optimization are visible. The original blowing pattern has a significantly higher area of excessive chromium compared to the optimized control strategy. Once again, the area between the blue se-

ries and the red series is the excessive oxygen, which reacts with chromium based on the kinetic decarburization approach. In terms of numbers, this means 168 m^3 O_2 dedicated to chromium in the original pattern and 108.9 m^3 O_2 dedicated to chromium in the optimized pattern. This underlines a clear theoretically based optimization of the control strategy.

Although the simulations and tests of the optimization clearly show enhanced control strategies regarding the objective function, the interpretation and moreover the conclusion must be stated carefully. Notably, the generated pattern does not have real-time data in the background for simulation. In particular the system pressure simulation shows the highest basis for argumentation. Since the equipment is not able to reduce the pressure from one second to another, the effect of the pressure reduction for the generated pattern simulation might be slower in a real operation scenario. Also in terms of the oxygen injection rate, the equipment is not 100% able to follow set-points within a $\Delta t = 1$. Nonetheless, as pointed out with the numerical tests and simulations of the present section, there is a clear tendency for lower chromium oxidation by using a blowing pattern with a step-wise reduction at the end. However, as already pointed out during the discussion of the results, the step-wise reduction at the end leaves room for improvement of the algorithm. Furthermore, the more phenomena will be considered in the online model in the future, the better the transformation to an optimization algorithm can be.

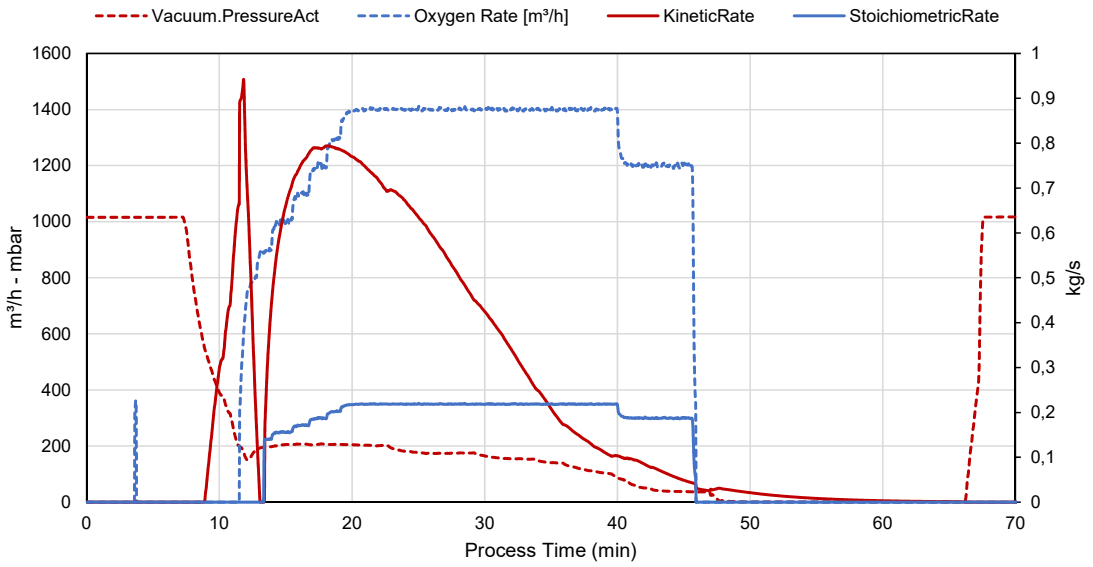

Figure 5.2: Original blowing pattern and results of the model

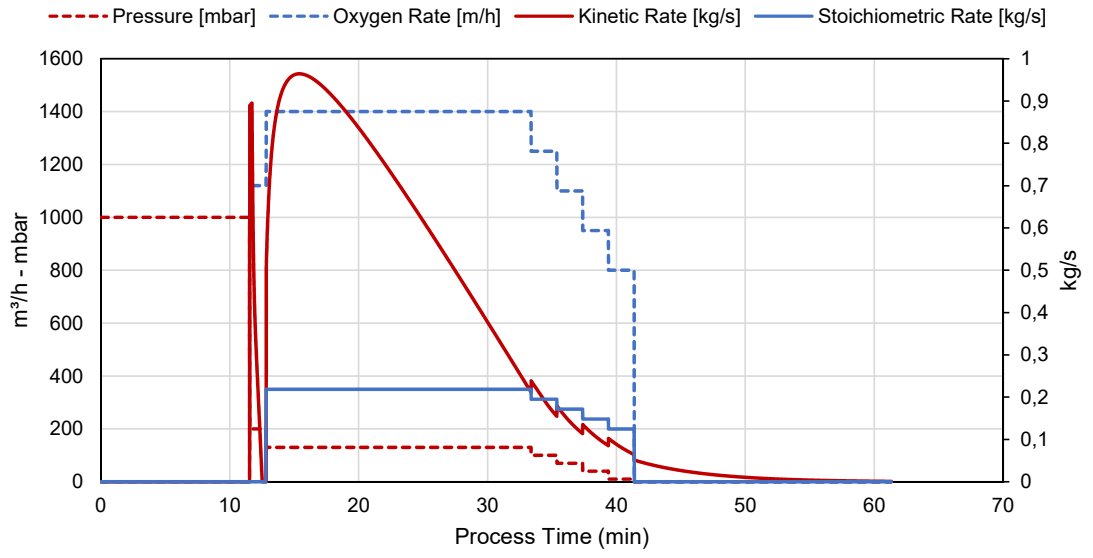

Figure 5.3: Generated blowing pattern and simulation the model of the 4-step solution

6 Conclusions

The present chapters provides comprehensive conclusions about the thesis and moreover a concluded discussion regarding the thesis' statement and its hypotheses. Based on an existing process model, which is validated and accepted in the field, the present thesis pointed out possible optimization potentials for the vacuum oxygen decarburization (VOD) process. By doing so, the thesis showed the influences of the oxygen injection rate, the system pressure and the stirring gas rate on the model result. Therefore, the present chapter is split into a summary of the methodology as well as a discussion of the results. Finally, an outlook for further researches, in the field of modeling and VOD operation, is provided based on the findings of the present thesis.

6.1 Summary

The VOD process is one of the most important methods in modern stainless steelmaking. Based on experience and observations in the field, it can be stated that different treatment strategies for the VOD operation influences the result of chromium-oxidation. Although the main purpose of a VOD operation during the steelmaking route is decarburization, the oxidation of chromium is an unwanted side-effect. The term decarburization means the removal of carbon in the liquid metal. In fact, extremely low carbon contents down to 0.005% in the presence of high chromium concentrations in the metal bath will be achieved. At this point, the mentioned drawback of oxidizing chromium during the oxidation has to be noted again. This negative effect is unwanted, because the recovery of chromium by the addition of so called reduction-materials is cost related and consequently expensive (Fruehan, 1998).

According to an existing VOD process model, validated and accepted in the field, the thesis examines and shows the effects of different control strategies on the results of

the model, especially the chromium oxidation. This research is the basis to describe the optimization potentials for the process. Importantly, the optimization potential is always regarding the results of the process model. For the sake of understanding the existing process model, the related work of the thesis provided a detailed introduction into the field of metallurgy, modelling and a comprehensive description of the setup of the model. Based on this related work and background information, the definition of an optimization problem is the first step. The mathematical problem statement is the key part for all further studies of the thesis. At next, a detailed variable study is carried out, examining the effects of the different variables defined in the optimization study. Finally, an optimization algorithm is then implemented by using the findings and results of the variable study. The following parts describe the methodology and results in detail.

Mathematical Problem Statement

The first major part of thesis is the examination of the existing model. Thus, an optimization problem has been set up with the chromium minimization as the objective function. Therefore, the following main points of an optimization problem are covered:

- Constants
- Input parameters
- Variables
- Objective function
- Constraints

The constants consist of physical and chemical constants on the one hand, and on the model tuning parameters on the other hand. The latter are taken from the commissioning of a VOD equipment at a disclosed customer in South Korea. The input parameters are defined as the steel and slag chemical composition as well as steel and slag weight. The variables, and as such the changeable set of data, are directly related to the blowing-pattern of the VOD process. Accordingly, the variables are the system pressure, the oxygen blowing rate and the stirring gas rate.

The objective function is set up to minimize the chromium content according to the mathematical expressions of the model. With respect to the formulations, the objective function

consists of two parts: the first part is the amount of oxygen reacting with chromium by the constant distribution $\mathrm{R_{Cr}}$; the second part covers the left-over oxygen of the decarburization whenever the kinetic approach is in favor.

At last, the optimization must meet some constraints. The constraints are mostly based on the knowledge of relevant papers, textbooks and experience of metallurgists. As an example, the initial oxidation phase of priority elements must be carried out at 80% of the maximum flow rate to avoid heavy boiling and splashing. In other words, to protect the equipment and operate the process safely. Also the system pressure at the main phase is limited due to safe operation and capability issues.

Variable Study

The fundamental description of the optimization problem serves as basis for a variable study. Thus, an initial illustrative numerical example is carried out to explain every calculation step in detail. This means, the example illustrates the conduction of the objective function and its result step by step. The numerical illustration shows already the comparably low influence of stirring gas on the result. Of course it has to be mentioned again, the negligible effect of the bottom stirring is observed based on the formulation of the existing model. However, the existing process model does not account the influence of stirring gas for the reaction interface. Besides, every carried out calculation of the variable study is executed at the same conditions (input parameters of the illustrative example).

At first, the influence of the oxygen injection flow turned out to be limiting. The introduction of steps as the final blowing phase shows improved results, although the enhancements are smaller the more steps are introduced. The seen effect is based on the necessity of extending the blowing pattern to reach the target carbon content and temperature before the boil-off phase. At last, by reducing the system pressure together with the oxygen flow, further improvements have been achieved in the results. The last example of the effect study of variables shows the best result: four final blowing steps performing the reduction of oxygen blowing and system pressure at the same time. The figures of interest are 171.80 m^3 O_2 for the initial blowing pattern (illustrative example), while the final variable setup shows 108.86 m^3 O_2 reacting with chromium according to the model.

Optimization Algorithm

Based on the outcome of the variable study, an optimization algorithm has been implemented. In general, the algorithm incorporates the correlation observed in the last result

of the study: a step-wise reduction concept at the final blowing phase. Thus, the algorithm calculates the reduction of oxygen and system pressure based on the number of steps. Firstly, the algorithm is tested with the same conditions as the variable study at a number of 104.37 m^3. Although following the same concept, the programmatic algorithm could improve the manual solution. The same algorithm is tested with slightly modified input parameters. These examples are based on the initial parameters but modified in terms of the start carbon content. By doing so, the results of the algorithm show a similar result for a similar start carbon content. The high carbon steel shows a reasonable higher figure. However, the final chromium content after boil-off is comparably high. This means a lower chromium oxidation as it can be observed with lower carbon contents. As discussed, the kinetic decarburization rate depends on the system pressure as well as the temperature. And since the high carbon steel gains more temperature due to the carbon oxidation, the less chromium is oxidized overall based on the higher kinetic rate. Exactly the opposite has been pointed out with a low carbon steel at a level of 0.200% C. The combination of the low temperature of 1590 °C together with less carbon to gain temperature, the chromium oxidation is as expected higher. Even higher than the initial parameters, with a carbon concentration of 0.400%.

Finally, a comparison of an optimized control strategy based on the implemented algorithm with process data carried out in the field shows the improvements achieved in the thesis. This effect is visually supported by diagrams, showing the area of excessive oxygen notably higher in the original pattern compared to the model-based optimized control strategy.

6.2 Outlook

The present master's thesis points out the critical part of the VOD operation. An obviously high chromium oxidation happens, whenever the critical carbon point is reached and the excessive oxygen favors the chromium reaction. Consequently, a step-wise reduction of the oxygen blowing rate at the end of the process leads to lower chromium oxidation. But, as also pointed out, the oxygen blowing rate only does not have the same effect as it has together with the pressure reduction. Therefore, the final optimization step defines a combined reduction of oxygen and pressure. However, the developed optimization algorithm of the thesis is defined by assumptions based on the experience of the company.

To overcome the lack of assumptions when generating a blowing pattern, further investigations about the capabilities of such equipment can help to further improve blowing patterns. Since the results show that the reduction of the pressure after the critical carbon content has a strong influence, the capability of the vacuum pumps is the one of interest.

Nevertheless, the thesis introduces the first optimization algorithm to create oxygen blowing patterns, which is based on a mathematically defined optimization problem. The optimization problem itself is defined on the basis of the existing model as described. This leads to the following possibilities for further investigations and improvements: (1) on the one hand, the newly developed algorithm leaves room for enhancements; (2) on the other hand, the model where the optimization problem is conducted from is open to comprise more physical phenomena in the future.

Clearly, the model itself and the algorithm to generate blowing patterns are - and must be - closely tight together. This means, the better the model the better the outcome of any optimization. For example, the beginning of the generated blowing pattern is defined to be static at certain oxygen flow rate. The definition of 80% of the maximum blowing rate is based on the assumption of boiling and splashes, as already mentioned above. Nonetheless, the more knowledge and further research is available the more constraints for the optimization problem can be defined. As a consequence, any optimization algorithm to generate blowing patterns can be extended to cover more fundamental based constraints. As a next step, the introduced Gibbs minimization to distribute the oxygen already at the beginning of the blowing phase, can be introduced into the existing model and therefor also into the optimization algorithm. Another field of interest is the conduction of the so-called carbon removal efficiency or as it is introduced in the thesis: the β factor. This factor mainly defines the efficiency of the kinetic. To overcome the lack of two single parameters in the model, further researches may help to define this important factor based on other fundamental-based ideas, like describing the CO and Ar bubble behavior.

List of Figures

List of Tables

List of Algorithms

Bibliography

AZoM. (2001). *Stainless steel - grade 316 (uns s31600).* https://www.azom.com/article.aspx?ArticleID=863. (Accessed: 2017/12/11)

Björkvall, J. (2000). Trita-met 070. *Division of Metallurgy, Dept. of Materials Science and Eng., Royal Institute of Technology, Stockholm, Sweden*.

British Stainless Steel Association. (n.d.). *History of stainless steel: 1980 - present.* http://www.bssa.org.uk/about_stainless_steel.php?id=164. (Accessed: 2017/10/18)

Brooks, G., Dogan, N., Alam, M., Naser, J., & Rhamdhani, M. (2011). Developments in the modelling of oxygen steelmaking. *Faculty of Engineering - Papers*.

Brooks, G., Rhamdhani, M., Coley, K., & Pan, Y. (2009). Transient kinetics of slag metal reactions. *Metallurgical and Materials Transactions B*, *40*(3), 353–362.

Buchdahl, H. A. (2009). The concepts of classical thermodynamics. *The Concepts of Classical Thermodynamics, by HA Buchdahl, Cambridge, UK: Cambridge University Press, 2009*.

Çamdali, Ü., & Tunç, M. (2006). Steady state heat transfer of ladle furnace during steel production process. *Journal of Iron and Steel Research, International*, *13*(3), 1825–20.

Choudhury, A., Bruckmann, G., & Scholz, H. (1988). Computerized control of the vod process with the application of a mass spectrometer. *Metall. Plant Technol.*, *11*(5), 44.

Davies, R., & Taylor, G. (1950). The mechanics of large bubbles rising through extended liquids and through liquids in tubes. In *Proceedings of the royal society of london a: Mathematical, physical and engineering sciences* (Vol. 200, pp. 375–390).

Deo, B., & Boom, R. (1993). *Fundamentals of steelmaking metallurgy*. Prentice-Hall.

Díaz, M. C., Komarov, S. V., & Sano, M. (1997). Bubble behaviour and absorption rate in gas injection through rotary lances. *ISIJ international*, *37*(1), 1–8.

Ding, R., Blanpain, B., Jones, P. T., & Wollants, P. (2000). Modeling of the vacuum oxygen decarburization refining process. *Metallurgical and Materials Transactions B*, *31*(1), 197–206.

Ekengård, J. (2004). *Aspects on slag/metal equilibrium calculations and metal droplet characteristics in ladle slags* (Unpublished doctoral dissertation). Materialvetenskap.

Ellingham, H. J. T. (1944). Reducibility of oxides and sulfides in metallurgical processes. *J Soc Chem Ind*, *63*, 125–133.

Eriksson, G. (1975). Thermodynamic studies of high-temperature equilibria. 12. solgasmix, a computer-program for calculation of equilibrium compositions in multiphase systems. *Chemica Scripta*, *8*(3), 100–103.

Frohberg, M., & Kapoor, M. (1978). Thermodynamic models of slags. *Physical Chemistry and Steelmaking.*, *2*, 2.

Fruehan, R. J. (1998). *The making, shaping and treating of steel, vol. 2: Steelmaking and refining volume* (11th Edition ed.). Pittsburgh, PA: AISE Steel Foundation.

Gaskell, D. R. (2008). *Introduction to the thermodynamics of materials*. CRC Press.

Gaye, H., & Coulombet, D. (1984). *Pcm re.1064, ceca no 7210 – cf/301*. Institut de Recherches de la Sidérurgie Française.

Gaye, H., Lehmann, J., Rocabois, P., & Ruby-Meyer, F. (2001). Computational thermodynamics and slag modelling applied to steel elaboration. *steel research international*, *72*(11-12), 446–451.

Ghosh, A. (2000). *Secondary steelmaking: Principles and applications*. CRC Press.

Gmelin-Durrer, Trenkler, H., & Krieger, W. (1984). *Metallurgy of iron: Practice of steelmaking 1. pt. b. illustrations*. Springer.

Gordon, S., & McBride, B. J. (1994). *Computer program for calculation of complex chemical equilibrium compositions and applications* (Vol. 1). National Aeronautics and Space Administration, Office of Management, Scientific and Technical Information Program.

Gupta, N., & Chandra, S. (2004). Temperature prediction model for controlling casting superheat temperature. *ISIJ international*, *44*(9), 1517–1526.

Hallberg, M., Jonsson, T. L. I., & Jönsson, P. G. (2004). A new approach to using modelling for on-line prediction of sulphur and hydrogen removal during ladle refining. *ISIJ international*, *44*(8), 1318–1327.

Heinen, K.-H. (1997). *Elektrostahl-erzeugung* (Vol. 4). Düsseldorf: Stahleisen.

Henry, W. (1823). *The elements of experimental chemistry* (9th ed., Vol. 1; W. Henry,

Ed.). Baldwin, Cradock and Joy, and R. Hunter.

Himmelblau, D. M., & Bischoff, K. B. (1968). *Process analysis and simulation: deterministic systems*. Wiley.

Kitamura, S.-y., Yano, M., Harashima, K., & Tsutsumi, N. (1994). Decarburization model for vacuum degasser. *Tetsu-to-Hagané*, *80*(3), 213–218.

Kitamura, T., Miyamoto, K., Tsujino, R., Mizoguchi, S., & Kato, K. (1996). Mathematical model for nitrogen desorption and decarburization reaction in vacuum degasser. *ISIJ international*, *36*(4), 395–401.

Kleimt, B., Lichterbeck, R., De Angelis, V., De Paolis, G., Rinaldi, M., Sabatini, G., & Burkat, C. (2006). Improvement of process control and refractory performance of the aod converter. *EUR*(21974), 1–120.

Kuwabara, T., Umezawa, K., Mori, K., & Watanabe, H. (1988). Investigation of decarburization behavior in rh-reactor and its operation improvement. *Transactions of the Iron and Steel Institute of Japan*, *28*(4), 305–314.

Lindenberg, H., Schubert, K., & Zörcher, H. (1987). Entwicklung der schmelzmetallurgie nichtrostender stähle. *Stahl und Eisen*, *107*, 1197–1204.

Lytvynyuk, Y., Schenk, J., Hiebler, M., & Sormann, A. (2014). Thermodynamic and kinetic model of the converter steelmaking process. part 1: The description of the bof model. *Steel research international*, *85*(4), 537–543.

Mayer, M., Pfennig, M., Weigl, A., & Pierer, R. (2017). Challenges and capabilities in software development for fundamental-based on- and offline simulation of metallurgical processes. In *Proceedings of the 9th international conference of young scientists on welding and related technologies* (pp. 25–33). Kyiv: WRTYS.

Mazumdar, D., & Evans, J. W. (2009). *Modeling of steelmaking processes* (1st Edition ed.). Boca Raton, Fla: CRC Press.

Ohta, H., & Suito, H. (1998). Activities of sio 2 and al 2 o 3 and activity coefficients of fe t o and mno in cao-sio 2-al 2 o 3-mgo slags. *Metallurgical and Materials Transactions B*, *29*(1), 119–129.

Otto, J. (1976). Variation of concentrations in high chromium steels at vacuum refining and process monitoring by continuous measurement of oxygen partial pressure in the offgas. *Stahl u. Eisen*, *96*(20), 939–945.

Patil, B., Chan, A., & Choulet, R. (1998). Chapter 12: Refining of stainless steels. *The Making, Shaping and Treating of Steel, Steelmaking and Refining Volume, 11th ed., RJ Fruehan, ed., AISE Steel Foundation, Pittsburgh*, *11*, 716–741.

Reichel, J. (1996). *Optimisation of decarburisation of high chromium steels* (Unpublished

doctoral dissertation). Academy of Mining and Metallurgy, Cracow.

Reichel, J., & Szekely, J. (1995). Mathematical models and experimental verification in the decarburization of industrial scale stainless steel melts. *Iron & steelmaker*, *22*(5), 41–48.

Rodríguez-Hernández, H., Garnica-González, P., & JA, R.-S. (1997). A mathematical model for the reduction kinetics of iron oxide in electric furnace slags by graphite injection. *ISIJ international*, *37*(11), 1072–1080.

Schürmann, E., & Rosenbach, K. (1973). Herstellung von niedriggekohlten, nichtrostenden austenitischen chrom-nickel-stählen nach dem argon-sauerstoff-entkohlungsverfahren. *steel research international*, *44*(10), 761–768.

Sourcebook, S. D. (1988). by the 19th committee on steelmaking. *JSPS, Gordon and Breach Sci. Pub., Montreux*, *59*.

Tian, H., Mao, Z., & Wang, Y. (2008). Hybrid modeling of molten steel temperature prediction in lf. *ISIJ international*, *48*(1), 58–62.

Turkdogan, E., & Fruehan, R. (1998). Fundamentals of iron and steelmaking. *The Making, Shaping and Treating of Steel, Steelmaking and Refining Volume, 11th ed., RJ Fruehan, ed., AISE Steel Foundation, Pittsburgh*, 125–126.

Turkdogan, E. T. (1996). *Fundamentals of steelmaking* (Vol. 614). Maney Pub.

Wagner, C. (1952). *Thermodynamics of alloys* (Tech. Rep. No. 546.3015367). Boston: Addison-Wesley Press.

Wei, J.-H., & Li, Y. (2015). Study on mathematical modeling of combined top and bottom blowing vod refining process of stainless steel. *steel research international*, *86*(3), 189–211.

Wei, J.-H., & Zhu, D.-P. (2002). Mathematical modeling of the argon-oxygen decarburization refining process of stainless steel: Part i. mathematical model of the process. *Metallurgical and materials transactions B*, *33*(1), 111–119.

Wulandari, W., Brooks, G. A., Rhamdhani, M., & Monaghan, B. J. (2009). Thermodynamic modelling of high temperature systems. *Engineering Our Future: Are We up to the Challenge?: 27-30 September 2009, Burswood Entertainment Complex*, 382.

Xiao, Y., & Holappa, L. (1993). Determination of activities in slags containing chromium oxides. *ISIJ international*, *33*(1), 66–74.